

Design and Modeling of Bio-Inspired Shoulder Exoskeleton with Cable-Driven Quasi-Direct Drive Actuation: Misalignment Compensation and Interference Mitigation

Abstract—Powered shoulder exoskeletons can decrease shoulder loading and reduce work-related injury risk. However, they face two major challenges: (1) providing effective torque assistance without misalignment or impeding natural shoulder movement, and (2) simultaneously satisfying portability and high torque density. To address these challenges, first, inspired by the kinematics of the human scapula, we designed a self-aligning mechanism that mimics human scapular rotation and protraction to assist shoulder abduction and flexion while avoiding joint misalignment. We also developed a variable lever arm mechanism that effectively reduced the size of the structure moving with the upper arm to mitigate the interference between robot and natural shoulder movement. Second, we developed a lightweight, portable shoulder exoskeleton with cable-driven quasi-direct drive (C-QDD) actuation, which provides partial biological torque assistance with high torque density. We derived the kinematics model and state-space model of human-exoskeleton interaction to characterize the system dynamics and inform future controller design. Results showed that (1) with a unilateral weight of 1.9 kg, our shoulder exoskeleton can deliver up to 13 Nm torque for assisting shoulder abduction and flexion, achieving the most lightweight and highest torque density among portable shoulder exoskeletons. Human experiments ($n=7$) showed that (2) our exoskeleton has minimal interference with natural shoulder movement with the lowest reduction (<8%) in the range of motion when wearing the exoskeleton, and (3) achieved the highest net reductions (-23.9% to -65.2%) in average muscle activation during three activities and significant increase (54.1% to 73.2%) in endurance time for holding task.

Index Terms—Shoulder exoskeleton, biomimetic mechanism design, human-robot misalignment, cable-driven quasi-direct-drive actuation.

I. INTRODUCTION

Shoulder exoskeletons offer a promising solution to restore upper limb functionalities and lower the risks of work-related musculoskeletal injuries [1], [2]. They also have the potential to improve employment opportunities for people with certain disabilities [3], [4]. To date, most developments on upper limb wearable robots have predominantly focused on rehabilitation devices, which are designed to facilitate arm function recovery through specific therapeutic training by providing full actuation and maximum joint torque support [5]–[8]. However, there is a lack of assistive shoulder exoskeletons that aim to provide partial torque assistance for people with residual strength to achieve immediate functional support. Unlike rehabilitation devices, assistive shoulder exoskeletons must provide effective joint support while avoiding misalignment and minimizing interference with natural motion.

Moreover, shoulder exoskeletons must be fully portable, and lightweight for practical use in unstructured environments, including home use. These multifaceted requirements pose unique design challenges in assistive shoulder exoskeletons.

The first challenge in assistive shoulder exoskeletons is to provide effective torque assistance while simultaneously avoiding joint misalignment and minimizing physical interference between robot and natural human shoulder movements. Misalignment occurs when there is a mismatch between the rotational centers of the exoskeleton's mechanical joint and the user's anatomical joint, which can generate unwanted interaction forces and lead to ineffective assistance [9]. Interference refers to any physical obstruction that restricts shoulder motion. The shoulder joint is one of the most mobile joints in the human body [10], [11], functioning as a ball-and-socket joint with three rotational degrees of freedom (DOFs): flexion/extension, abduction/adduction, and internal/external rotation. Functional upper limb movements involve coordinated motion of the scapula and clavicle, which shifts the shoulder joint's center of rotation dynamically during movement, and enables a large range of motion of the upper limb [12]. Accordingly, the device must both compensate for shifts of the joint center, thereby preventing misalignment and minimize interference arising from the mechanism's motion with the arm, thereby preserving natural shoulder movement. However, the anatomical complexity and mobility of the human shoulder joint make this requirement challenging.

State-of-the-art studies have attempted to tackle this issue, but still have their limitations. Rigid shoulder exoskeletons install actuators parallel to the shoulder joints [18]–[21] and may incorporate rigid misalignment compensation mechanisms [13], but require precise joint alignment and typically employ bulky frames that can significantly restrict the user's natural shoulder movement. For example, the designs of [22] and [23] caused significant physical interference between the robot and the human body, resulting in reductions of more than 32% and 35% in the range of motion of shoulder flexion and abduction, respectively, compared with the no exoskeleton condition. To mitigate the loss of natural shoulder range of motion when wearing an exoskeleton, the mechanism of shoulder exoskeleton must coordinate the kinematics of both humeral and scapular motion. While [7] addressed this challenge by adding redundantly actuated degrees of freedom at the user's clavicle to preserve scapulohumeral rhythm, but this increased complexity and resulted in a tethered system. Soft

TABLE I
BENCHMARK COMPARISON OF MECHATRONIC PERFORMANCE OF POWERED SHOULDER EXOSKELETONS: OUR ROBOT ACHIEVES THE MOST LIGHTWEIGHT AND HIGHEST TORQUE DENSITY

Powered Shoulder Exoskeleton	Structure	Bilateral Mass [†] (kg)	Unilateral Mass [†] (kg)	Actuation Paradigm	Portability	Assistive Torque (Nm)	Gear Ratio	Torque Density (Nm/kg)
This work	Hybrid	3.3	1.9	Cable-driven + QDD	Untethered	13	6:1	6.84
IIT [13]	Rigid	6.4	N.A.*	Low-torque motor + harmonic drive reducer	Untethered	~11	<u>100:1</u>	<3.44
Harvard [14]	Soft	N.A.*	>3.4	Pneumatic	Untethered	6.5	N.A.	<1.91
ETH [7]	Rigid	N.A.*	>10.5	SEA	Tethered	77	<u>100:1</u>	N.A.
WHU [15]	Rigid	N.A.*	N.A.*	SEA + cable driven	Tethered	33	101:1	N.A.*
NUS [16]	Rigid	4.5	~2.5	BLDC motor + SEA + cable-driven	Untethered	10	N.A.*	4
ETH [17]	Soft	N.A.*	N.A.*	Low-torque motor + gearbox + cable driven	Tethered	N.A.*	26:1	N.A.

[†]Overall mass including battery and electronics. *This article did not present this specification of their exoskeleton. In [7], actuators weighing 10.5 kg were proposed; In [14], portable actuation units weighing 3.4 kg were proposed; In [13], unilateral exoskeleton weight was not reported, but it is heavier than 3.2 kg; Abbreviation: N.A. = Not available. [should the 101:1 gear ratio also be underlined here?]

textile-based cable-driven shoulder exosuits [24]–[26], which employ cable systems to achieve a tendon-driven mechanism for assistance delivery and rely on the user's body as the robot frame **have also been proposed**. Although this design allows shoulder movements without misalignment, the cable tensions apply shear and normal compressions on the human upper limbs [25], [26], which can restrict the arm's natural motion (e.g., the exosuit in [17] reduced shoulder range of motion by more than 20%). Pneumatic exosuits [14], [27], [28] can elevate the upper arm by inflating balloon chambers under the armpit. This design can avoid compressing the joint as the balloon actuator pushes the limb away from the torso. However, since the assistance is applied to the flexible structure directly, the force can be easily misdirected due to the deformation of the balloon's soft transmission. This can lead to inefficient force transmission and malfunction. The same issue also exists in exoskeletons using a ball joint [16], [29] to connect the rigid skeleton and the human waist, where the assistance can be misdirected during the user's arm movement due to the excessive flexibility of the ball joint.



Fig. 1. The bio-inspired, lightweight powered shoulder exoskeleton with cable-driven quasi-direct-drive (c-QDD) actuation integrates (i) a biomimetic self-aligning mechanism and (ii) a variable lever-arm mechanism (see Method 1), a carbon-fiber frame, textile wearables, and two c-QDD actuation units. Total mass: 1.9 (3.3) kg, including control electronics and a 0.5 kg battery. Design details are illustrated in Fig. 2 and Fig. 3.

The second challenge in assistive shoulder exoskeletons is delivering sufficient torque assistance (30–50% biological

torque) **Needs justification here why 30-50 percent of the torque** while remaining a lightweight design. Prior studies [2], [30] have shown effective assistance by providing small to medium level torque support. However, state-of-the-art shoulder exoskeletons cannot simultaneously achieve human-scale torque output and lightweight design due to inherent limitations in their actuation paradigms. Passive shoulder exoskeletons provided a portable solution for industrial applications to augment the performance and safety of workers for repetitive or strenuous tasks in the workplace [31]–[33], by using spring-based mechanisms to generate assistive torque [34]–[36]. However, their design methods remain unknown as there is no theoretical study analyzing the mechanism design principle. [This last sentence seems odd to me. What does it mean for design methods to be unknown? To me seems to mean that we don't know how they make them.] Moreover, a major limitation of passive shoulder exoskeletons is that their assistance profile is not controllable because their assistive torque is determined by the intrinsic properties of the elastic elements. Additionally, these passive exoskeletons require the user to store energy during some operations, such as lowering the arm, **making it challenging for individuals with arm weakness to use and potentially causing muscle fatigue, limiting their applicability in broader scenarios like daily living**. As opposed to passive ones, one major advantage of powered shoulder exoskeletons or exosuits is their ability to provide external energy through controlled assistance profiles that dynamically adapt to the user's effort.

State-of-the-art powered shoulder exoskeletons can be classified into three main groups based on their actuation paradigms, which include 1) conventional low-torque motors with high gear ratio reducers-based exoskeletons or soft exosuits, 2) series elastic actuators (SEA)-based exoskeletons, and 3) pneumatically actuated exosuits. Each of these approaches presents limitations that hinder their effectiveness in assistive applications. First, exoskeletons based on conventional low-torque motors require high-gear ratio reducers to achieve sufficient torque output due to the motor's low torque density limitation. This significantly increases the weight and bulk

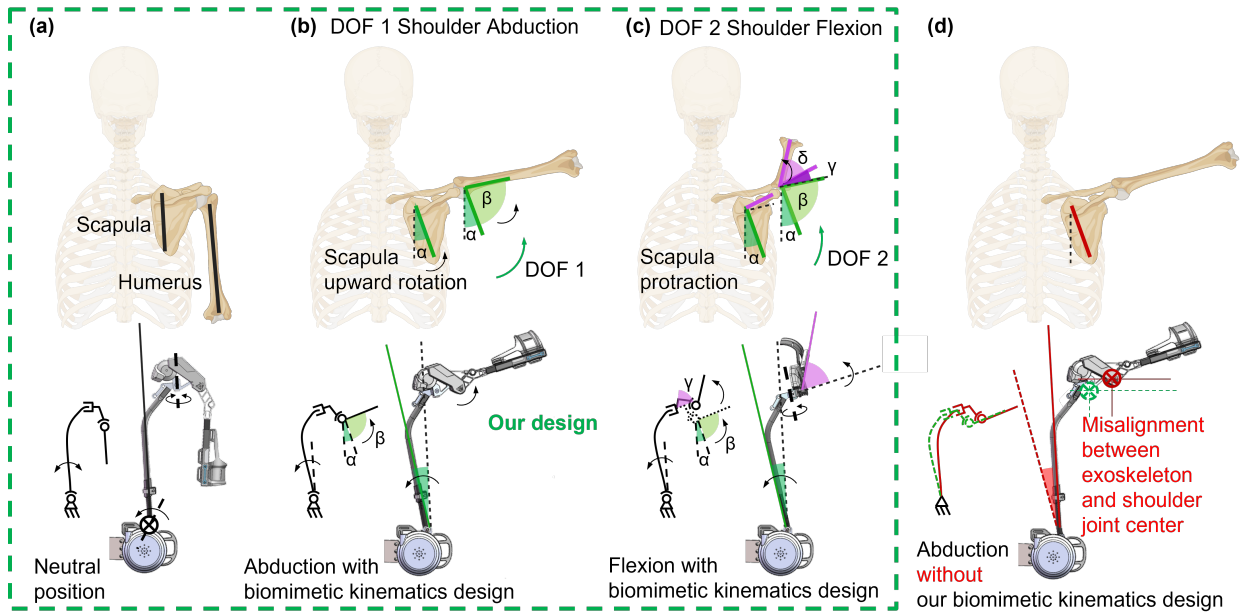


Fig. 2. Our bio-inspired shoulder exoskeleton provides powered assistance in abduction (DOF 1) and flexion (DOF 2) by mimicking scapular upward rotation and protraction to maintain joint alignment. A two-joint self-aligning mechanism with passive planar revolute joints enables this: (a) at neutral, the carbon-fiber rod and upper-arm link align with the scapula and humerus; (b) during abduction, the first joint lets the rod rotate inward in the frontal plane as the scapula rotates on the thorax; (c) during elevation/flexion, the second joint permits horizontal abduction/adduction, mimicking protraction and enabling DOF 2 assistance; (d) this bio-inspired design avoids robot–shoulder misalignment typical of rigid or ball-and-socket mechanisms.

of actuation and compromises compliance in human-robot interaction due to the large friction and high reflected inertia of their transmission, resulting in tethered designs [17] or bulky untethered systems (e.g., 6.4 kg total mass in [13]), making them unsuitable for daily assistive use. First, low-torque motors need high-gear reducers for sufficient output, but this increases weight, bulk, and transmission inertia, reducing compliance. Consequently, systems are often tethered [17] or heavy when untethered (e.g., 6.4 kg in [13]), making them impractical for daily assistive use. Second, while SEA-based exoskeletons can deliver high assistive torque with enhanced compliance, they are either tethered [7], [37] or heavy (e.g., 4.5 kg total mass in [16]) untethered robots due to the extra mass from added components, such as extra elastic components, sensors, and ball screws. Third, though pneumatically actuated exosuits [14], [38] can be portable and capable of providing small to medium torque assistance [28], they suffer from the low inflation speed and unavoidable hysteretic behavior due to the compressibility of air. This adds substantial complexity to the control strategy when trying to achieve agile assistance to enable fast response and seamless assistance [19]. Moreover, the use of air pumps generates significant vibrations and noise, making them not ideal for real-life applications. These limitations prevent state-of-the-art actuation paradigms from achieving both lightweight and human-scale torque assistance to satisfy the multifaceted demands of assistive upper limb wearable robots.

To address the first challenge of assisting shoulder movement without joint misalignment, while minimizing physical interference between the exoskeleton and natural shoulder movement, first, we propose a biomimetic mechanism inspired by human scapular kinematics. since the whole paper sort of focus on the idea of "bio-inspired", would be great to have a comparison figure on the bio-mechanism vs designed

exo mechanism - similar to the one in the video presentation attached The human scapula is a critical anatomical structure that stabilizes the shoulder joint and facilitates extensive arm mobility. During shoulder abduction, the scapula rotates along the thoracic cage, enhancing mobility and ensuring alignment of the glenohumeral joint. Similarly, during shoulder horizontal adduction and flexion, the scapula protracts around the ribcage to extend the range of motion for forward-reaching movement. We designed a biomimetic mechanism to mimic the kinematics of scapula using two strategically positioned passive planar revolute joints to compensate for the misalignment between the exoskeleton and human shoulder (Fig. 5). Unlike the ball-and-socket mechanisms in [16], [29], which allow excessive unconstrained motion that can misdirect assistance, our planar revolute joint (Fig. 2) enabled the carbon-fiber linkages to freely rotate in the frontal plane or transverse plane, but without translation or shifting to other planes to prevent the malalignment issues. Second, to mitigate the physical interference between exoskeleton and human shoulder movement caused by the bulky structure moving with user's arm, we developed a variable moment arm mechanism to reduce the size of transmission mechanism on shoulder. Instead of using a fixed moment arm mechanism (usually a bulky fixed pulley and its frame [16], [39]) to transmit assistive torque to upper arm, we designed a winch-like variable lever arm mechanism that mechanically adjusts the assistive torque moment arm as shoulder elevates to address the needs of increasing biomechanical demand for assistive torque, while remaining a compact mechanism design (Fig. 3).

To address the second challenge of designing a fully portable, lightweight shoulder exoskeleton capable of delivering 30–50% biological torque assistance, we proposed the mechatronic design of cable-driven quasi-direct drive actuation (C-QDD) for shoulder exoskeleton and derived both

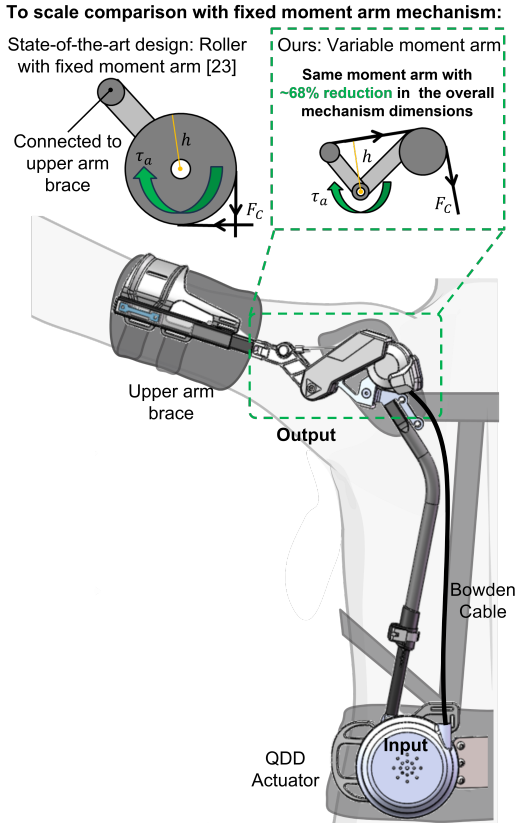


Fig. 3. Our variable assistive torque moment arm mechanism achieves the equivalent lever arm up to 71mm with 68% reduction of the volume of torque transmission mechanism moving with user's upper arm, compared to state-of-the-art fixed moment arm designs [16], [22], thus significantly reducing bulk and physical interference between robot and human movement. The assistive torque τ_a exerted on the user's shoulder joint equals the product of the cable's pulling force F_c , and the moment arm h , which varies as a function of the shoulder elevation angle.

the robot's kinematics and state-space model of the human-exoskeleton interaction dynamics. While quasi-direct-drive actuation has shown success in lower limb exoskeletons, no prior work has fundamentally investigated cable-driven QDD systems, and C-QDD has never before been implemented in a portable shoulder exoskeleton. Previous studies [40] demonstrated the feasibility of attaining high torque while maintaining a lightweight and portable design using a QDD actuation paradigm, which combines a high-torque motor with a low transmission ratio (less than 10:1). However, these efforts primarily focused on actuator design and lower limb assistance, where the QDD actuators are aligned laterally with the joints and transmit the torque to the user through a rigid frame. Such a rigid-framed configuration is not suited for the shoulder, which operates over multiple degrees of freedom and a significantly larger range of motion, and requires precise joint alignment that can make rigid systems bulky and burdensome for the upper limbs. In this study, for the first time, we created a portable, powered shoulder exoskeleton (Fig. 2 e) with a cable-driven-QDD actuation that can provide unilateral or bilateral torque assistance at the shoulder, and derived bottom-up kinematic model and state-space model of the shoulder exoskeleton to characterize the human-robot interaction dynamics and inform mechanical and

future controller design.

The contribution of this work is focused on the design and modeling of a lightweight bio-inspired shoulder exoskeleton with self-aligning and variable lever arm mechanisms, aimed at addressing joint misalignment, mitigating physical interference between robot and natural shoulder movement, and providing torque assistance via high-torque-density cable-driven quasi-direct drive (C-QDD) actuation. First, we proposed a biomimetic mechanism design that mimics human scapular kinematics to avoid misalignment between robot and human shoulder joint and designed a variable lever arm mechanism to reduce mechanical bulk. Our mechanism designs enabled assistance for both shoulder flexion and abduction while minimizing physical interference between the robot and natural shoulder movement. Second, we designed a portable, lightweight shoulder exoskeleton with C-QDD actuation, modeled its kinematics to inform exoskeleton mechanical and controller design, and derived the state-space modeling to characterize the human-exoskeleton interaction dynamics. This is the first work to design and model such a robot since C-QDD actuation had not previously been designed for a portable shoulder exoskeleton.

II. HUMAN SHOULDER BIOMECHANICS AND DESIGN REQUIREMENTS FOR SHOULDER MOVEMENT ASSISTANCE

Understanding the biomechanics of the human shoulder joint is essential for defining the design requirements of a portable assistive shoulder exoskeleton. However, it remains unclear how to design a portable assistive shoulder exoskeleton that can effectively provide partial torque support for both non-disabled users, such as workers, and individuals with shoulder impairments who retain residual muscle strength, without joint misalignment and interference with shoulder movement. In this study, first, we define that our robot must be able to effectively assist shoulder flexion and shoulder abduction, and enable free horizontal adduction and abduction while the shoulder is being lifted without joint misalignment. Second, to minimize physical interference between the robot and the user's natural shoulder movement, the structure that moves with the upper arm must be compact, achieving design simplicity (less is more). Last, the robot must be fully portable and lightweight so that it can be worn and carried around to assist with various activities.

A. Biomechanics of Human Shoulder Joint to Inform Shoulder Exoskeleton Design

As the most proximal joint in the upper limb's kinematic chain, human shoulder joint bears the highest torques against gravity [12]. It allows the arm to traverse approximately 65% of a spherical surface, providing the flexibility required for various functional tasks [41]. Its complex structure, comprising the scapula, clavicle, and humerus, allows for three primary degrees of freedom: flexion/extension (motion in the sagittal plane), abduction/adduction (motion in the coronal plane), and medial/lateral rotation (motion in the transversal plane). These movements are facilitated by the glenohumeral, acromioclavicular, sternoclavicular, and scapulothoracic joints, which work together to achieve dynamic stability and mobility.

The primary biomechanical functions of the shoulder joint include generating torques for arm elevation, maintaining static postures, and coordinating with the elbow and wrist for functional tasks. These functions are critical for activities of daily living, such as overhead work and lifting. Overhead work or static holding requires prolonged contraction of muscles, particularly the deltoid and trapezius to counteract gravitational torque. These muscles also play a stabilizing role, preventing dislocation in an inherently unstable joint complex. Their coordinated recruitment compensates for both gravitational and external loads (Table II).

The required biological torque of the shoulder joint is also influenced by the angle of arm elevation and the load being lifted. As the shoulder joint is elevated, the required torque becomes more significant. The estimated biological torque to fully sustain the arm of a male individual with a height of 1.75 m and a body mass index (BMI) of 25 is 11.5 Nm at 90° of shoulder elevation, based on a simplified kinematic model of the human arm and anthropometric data [42], [43]. Providing partial support during elevation can substantially reduce activation of the deltoid and trapezius, enabling prolonged activity and lowering the risk of musculoskeletal disorders (MSDs) such as rotator cuff injuries [12].

B. Design Requirements

Keep the sections title simpler Assistive shoulder exoskeletons must remain fully portable and lightweight to be worn and carried around and also to reduce the weight penalty of wearing the exoskeleton. Moreover, the structures moving with the human shoulder and upper arm should be compact and lightweight, thus to mitigate impacts on the inertial properties and physical interference between robot and user's natural movement. For our exoskeleton design, we aimed to provide partial (30-50%) biological torque assistance while ensuring a lightweight and compact form factor. Requirements are summarized in Table II.

Table format not consistent with the prior table - better follow the IEEE style

TABLE II
DESIGN PARAMETERS OF THE PARTIALLY ASSISTIVE SHOULDER EXOSKELETON

Parameter	Biological	Desired	This Work
Flexion range (°)	0–110*	0–110	0–180
Abduction range (°)	0–100*	0–100	0–180
Joint torque (Nm)	11.5	11.5	13
Joint velocity (rad/s)	1–2	2–3	3.97
Max joint speed (rad/s)	6.63	10	25
Exoskeleton weight (kg)	—	4	3.3

*Values denote the range of shoulder motion required for most activities of daily living [44].

Although it is unnecessary to provide assistive torque equivalent to full biological torque since partial assistive torques with right assistive timing can provide substantial biomechanical benefits to non-disabled individuals and people with impairments who still exhibit residual strengths to move

their arm [45], we designed our exoskeleton to provide more than 11.5 Nm assistive torque. This design choice allows the robot to assist in a broader range of activities, such as lifting different external loads, where the higher torque will help to compensate for gravitational torque caused by the weight of items to be lifted.

To mitigate the robot's interference with the user's natural shoulder movement, instead of aligning all the rotational centers of the human shoulder with the complex structure [7], [13], we proposed a compact and simple variable lever arm mechanism to effectively reduce the needed transmission mechanism size on user's shoulder.

III. BIOMIMETIC SELF-ALIGNMENT MECHANISM AND VARIABLE MOMENT ARM MECHANISM DESIGN TO MITIGATE PHYSICAL INTERFERENCE BETWEEN ROBOT AND NATURAL SHOULDER MOVEMENT

KEEP THE SECTION TITLES SIMPLE

IV. MECHANICAL DESIGN

Due to the complexity of the human shoulder anatomy and the coupled motions, state-of-the-art shoulder exoskeletons usually implement a bulky, rigidly framed design at the shoulder joint to align with each DOF and deliver assistance across a range of upper limb movements. Although such designs can provide effective torque support to human, they can easily cause joint misalignment and have to rely on control efforts or extra mechanisms to offset the misalignment. The bulky structure moving with human upper arm can also interfere with natural shoulder movement, resulting in a significant reduction in shoulder range of motion when wearing the exoskeleton. To address the misalignment issue and mitigate the physical interference between the robot and shoulder natural movement, we designed a biomimetic mechanism that mimics the human scapula kinematics to prevent misalignment and a variable lever arm mechanism to effectively reduce the torque transmission structure size moving with human shoulder.

A. Biomimetic Mechanism Design to Mimic Scapula Kinematics to Avoid Misalignment During Shoulder Movement

State-of-the-art shoulder exoskeletons commonly utilize rigid frames with fixed linkage lengths, neglecting the dynamic shift of the human shoulder's center of rotation during movement. This mismatch often leads to joint misalignment, causing unintended interaction forces and reduced effectiveness of torque assistance. To address this critical issue, we developed a biomimetic shoulder exoskeleton mechanism inspired by the kinematics of the human scapula, incorporating strategically positioned passive planar revolute joints. The human scapula contributes to shoulder joint stabilization and mobility. During shoulder abduction, the scapula rotates upward along the thoracic cage, thereby aligning the glenohumeral joint and enhancing the arm's elevation range. Similarly, during shoulder flexion and horizontal adduction, scapular protraction around the ribcage further extends the range of motion required for forward-reaching tasks. Drawing inspiration from these natural

movements, our exoskeleton integrates two passive planar revolute joints designed explicitly to mimic scapular rotation and protraction, ensuring precise alignment and effective assistance.

Specifically, the first passive revolute joint (Fig. 2 a), located near the user's waist, connects the rigid carbon fiber linkage to the waist belt. This joint allows the linkage to rotate inward within the frontal plane, closely replicating the upward rotation of the scapula as the user elevates their arm from a neutral position during shoulder abduction. This biomimetic movement prevents the misalignment commonly experienced in rigid exoskeleton designs by dynamically adapting the exoskeleton's orientation to match natural scapular rotation. The second passive revolute joint (Fig. 2 c) is positioned posteriorly at the shoulder level, connecting the carbon fiber structure to the upper arm support. This joint facilitates horizontal rotational freedom, mimicking scapular protraction and retraction. Thus, it enables the user to perform horizontal shoulder abduction and adduction movements naturally, utilizing their residual strength, even as the exoskeleton provides powered assistance in shoulder flexion.

By integrating these two passive joints with cable-driven quasi-direct drive (C-QDD) actuation, our exoskeleton effectively assists two primary shoulder degrees of freedom, i.e., shoulder abduction and flexion without misalignment between the robot and human shoulder. Unlike existing designs using ball-and-socket joints, our planar revolute joints constrain the exoskeleton's motion to specific anatomical planes, preventing excessive, unconstrained motion and thus significantly reducing joint misalignment issues.

B. Variable Lever Arm Mechanism Design to Mitigate Interference Between Exoskeleton and Shoulder Movement

Most of the state-of-the-art rigid shoulder exoskeletons directly place the actuator at the shoulder or surrounding the joint to minimize the misalignment. Such design enables effective torque assistance, but makes compromises in system bulkiness and interferes with natural shoulder movements. To facilitate the mechanism compactness, we designed a winch-like mechanism using a pulley and flexible hinge (Fig. 3), which enables the moment arm to increase as the shoulder joint is elevated, where higher assistive torque will be needed. The winch mechanism converts the cable pulling forces into rotational torque at the shoulder joint. In contrast to other shoulder exoskeletons that only deployed a rigid linkage bar connected to a roller with a fixed radius to transmit the assistive torque, our variable moment arm mechanism reduced the required mechanism dimensions by 68% and still provide the same moment arm of 71mm for assistive torque, thus effectively reducing the volume and weight moving with the user's arm. This reduction is calculated based on mechanical measurement of our robot, where the radius of pulley A is 21mm, the radius of pulley B is 6mm, and the radius of pulley C is 8mm, the area of linkage between pulleys A and B is 2646 mm^2 , and the area of linkage between pulleys B and C is 798 mm^2 , compared with a fixed pulley with radius of 71 mm. The reduction is calculated from mechanical measurements of our

robot, with pulley radii of 21 mm (pulley A), 6 mm (hinge B), and 8 mm (pulley C), linkage areas of 2646 mm^2 (A–B) and 798 mm^2 (B–C), compared to a fixed pulley of 71 mm radius. This variable lever arm mechanism effectively reduces system bulkiness and complexity, resulting in a more compact, simplified exoskeleton that enhances natural movement while providing the necessary support against gravity.

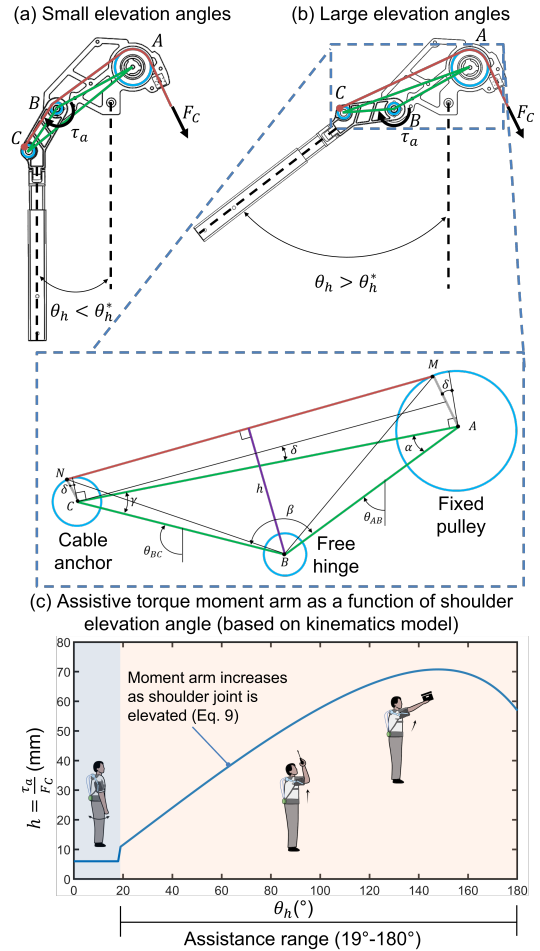


Fig. 4. The variable lever arm mechanism increases the assistive torque moment arm as shoulder elevation angle increases, effectively matching the joint's rising biological torque demand. (a) At small shoulder elevation angles (less than 19°), the moment arm equals the radius of hinge B, minimizing unwanted torque impeding natural arm swing. (b) At larger shoulder elevation angles, the moment arm increases as the cable moves away from hinge B. (c) The assistive torque moment arm is designed as a piece-wise function of shoulder elevation angle, based on Eq. 9. Our variable lever arm mechanism enables lever arm up to 71 mm at 150° elevation, effectively reducing the dimensions of needed mechanical components for torque transmission compared to the mechanism design with a fixed lever arm mechanism.

V. MECHATRONICS DESIGN OF SHOULDER EXOSKELETON WITH C-QDD ACTUATION

State-of-the-art assistive shoulder exoskeletons and exosuits cannot meet the multifaceted requirements of portability and high torque density simultaneously, due to the limitations of their actuation paradigms. The main objective of the proposed shoulder exoskeleton is to provide partial assistance for a broader range of activities with a new actuation paradigm that can address the limitations in the state of the art. This section details the mechanism design of the cable-driven quasi-direct

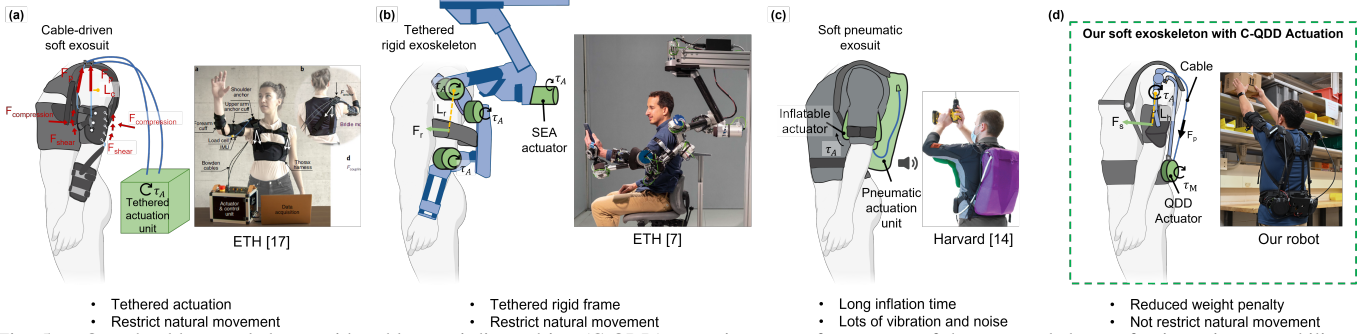


Fig. 5. Our shoulder exoskeleton with cable quasi-direct drive (C-QDD) actuation outperforms state-of-the-art exoskeletons for its unique capability to achieve both high torque density and portability. (a) Cable-driven exosuits rely on a tethered actuation unit [17] that is composed of low-torque motor with a high-gear ratio reducer and pulls the upper extremity directly to generate the assistance torque, which limits their application scenario. (b) Tethered rigid exoskeletons with series elastic actuators can provide high torque assistance by aligning actuators parallel to the human shoulder joints, but their heavy arm support structures and rigid frames significantly compromise portability [7], [18], [19]. (c) Portable pneumatic exosuit can be portable and provide torque assistance, but they suffer from low inflation speed and the use of air pumps generates significant vibrations and noise [47], limiting their practicality. (d) Our shoulder exoskeleton design leverages cable-driven transmission to reduce weight penalty by relocating mass to the waist, alongside high torque-density QDD actuation for portability.

driven (C-QDD) actuation paradigm and control electronics of the proposed shoulder exoskeleton.

A. Design of Cable Driven Quasi-Direct Drive (C-QDD) Actuation for Shoulder Exoskeleton

State-of-the-art actuators like the conventional actuators and SEAs are heavy and bulky because of the low-torque motors, reducers with a high gear ratio (e.g., harmonic drive with a gear ratio of 100:1 [46]) and elastic components, which causes large weight penalty for users and discomfort during long-term wearing, making them unsuitable for community or workplace-based use. Quasi-direct drive (QDD) actuators are more appropriate for assistive devices due to their high torque density motors, high compliance thanks to the low gear ratio reducers, and small moment of inertia. Cable transmission relies on Bowden cables and enables convenient placement of the actuator away from the distal joints. This remote actuation helps to reduce the inertial penalty on the user, promoting the simplicity and compactness of the device. The proposed cable-driven quasi-direct drive actuation of our shoulder exoskeleton consists of the actuator and the Bowden cable transmission, and the drive pulleys (Fig. 7). The actuator is composed of a high-torque motor with a low gear ratio planetary gearbox with a peak torque of 18 Nm (with a gear ratio of 6:1). The C-QDD actuation system operates between an input pulley connected to the actuator and an output pulley at the shoulder's end. A Bowden cable (Shinamo, steel coil outer sheath with ϕ 5mm, and ball-ended stainless steel inner cable ϕ 3mm-1.5m length, 10 kN max load) is used to transfer mechanical power from the actuation to the exoskeleton, which enables a convenient placement of the actuator away from the distal joint and thus minimizes the inertia on the arm. The actuator drives the input pulley (ϕ 52mm with 3mm groove, which converts the actuator torque into pulling forces in the cable. At the output end, the pulling force exerted on the cable pulls the carbon-fiber linkage bar, lifting the upper arm extremity with a fixed-pulley set as a winch mechanism, which converts rotation and force to the assistive torque.

The proposed shoulder exoskeleton consists of a rigid frame made of carbon tubes connected on one side to the waist belt

and on the other side to the shoulder joint lifting mechanism, which bears and transmits the weight from the upper arm to the human waist and ensures the effective torque transmission of the C-QDD actuation. The wearable components of the exoskeleton include textile-based components for comfort, magnetic V-buckles for quick connection and release, and length-adjustable frame and straps (Fig. 2) to ensure that the device can fit individuals with widely varying body types and sizes. Through the mechatronics design, we created the most lightweight portable powered shoulder exoskeleton (1.9 kg unilaterally, 3.3 kg bilaterally) with the highest torque density, delivering up to 13 Nm torque (Table I).

B. Control Electronics for Portable Shoulder Exoskeleton

The control electronics and a portable 22.2V Li-Po battery unit are packed on the waist belt, in between the two actuators. The control electronics are organized in a two-level architecture, as shown in Fig. 6. We used a Teensy 4.1 (Adafruit PJRC) as an embedded microcontroller unit for high-level control. It acquires human kinematics information from inertial measurement unit (IMU) sensors placed on the user's arms and sends the control command to the low-level torque controller of the QDD actuator embedded on its driver board through the Controller Area Network (CAN) bus communication, with a sampling frequency of 1 kHz. Two Bluetooth transceivers wirelessly stream data of in-situ assistive torque and human kinematics to a laptop with a graphic user interface (GUI) for visualization and monitoring. Moreover, the GUI allows for user control of the assistive level and assistance mode (unilateral or bilateral) can be adjusted and set in the high-level microcontroller unit. The microcontroller unit, IMU signal receiver, and robot-side Bluetooth transceiver are integrated into a compact custom PCB with a dimension of 85mm length by 100mm width. Through the battery, the PCB powers both the control electronics and two QDD actuators. It also transmits the torque command from the high-level controller to the actuator's low-level controller through the CAN cables. Per single charge, the battery life lasts about 3-4 hours, for bilateral use.

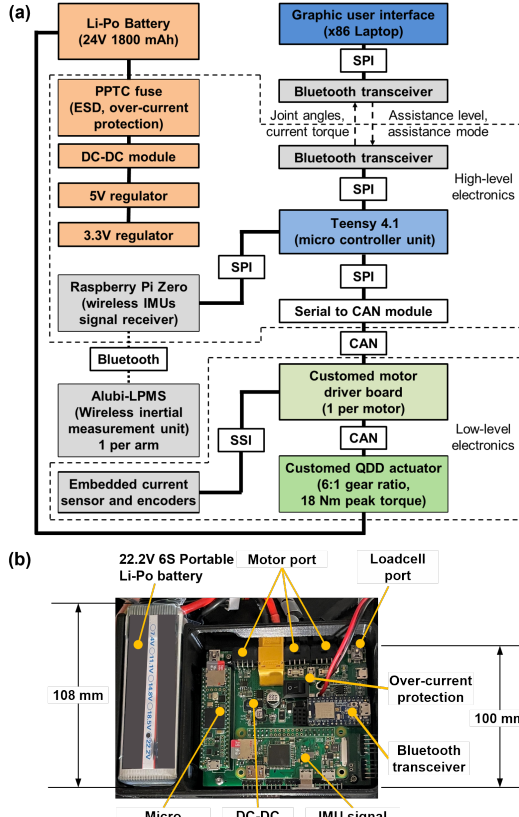


Fig. 6. Our compact portable electronics enable real-time communication for the shoulder exoskeleton (size: 85 mm *times* 100 mm). A Teensy 4.1 is used as a microcontroller unit for high-level control, which acquires human kinematics information from wireless inertial measurement unit (IMU) sensors and computes the desired torque commands. These commands are sent via the Controller Area Network (CAN) bus to the driver boards of the actuators, which run the low-level control to track the desired torque profiles with embedded encoders. Two Bluetooth transceivers wirelessly stream data of in-situ assistive torque and human kinematics to a laptop, which also enables adjustment in the assistance level and toggling between bilateral and unilateral modes. The total weight of the compact electronics control box is 500g (including a portable 22.2V Li-Po battery).

VI. KINEMATICS MODELING AND STATE-SPACE MODELING OF SHOULDER EXOSKELETON AND HUMAN-ROBOT INTERACTION TO UNDERSTAND THE NONLINEAR DYNAMICS AND SYSTEM CHARACTERIZATION

The human shoulder joint presents significant challenges for exoskeleton design due to its multiple degrees of freedom and the complex coupling of motions, which complicate exoskeleton controller design for torque assistance. To address these challenges, we aim to develop bottom-up kinematics and state-space modeling for characterizing the proposed shoulder exoskeleton dynamics and informing controller design. In this section, we modeled the kinematics of the system, and derived the state-space model of the human-exoskeleton interaction to characterize relationships between system input and output and provide a foundation for future model-based impedance controller design. Notably, this represents the first theoretical modeling effort for a shoulder exoskeleton employing C-QDD actuation, which was not previously studied for portable shoulder devices.

A. Kinematics Model of Shoulder Exoskeleton with Cable-driven Transmission and Variable Assistive Torque Lever Arm Mechanism

Modeling the kinematics of cable-driven shoulder exoskeletons presents unique challenges due to the nonlinear relationship between cable-driven actuator displacement and resulting joint motion, particularly when leveraging a variable assistive torque lever arm mechanism. Existing kinematic models for shoulder exoskeletons are primarily developed for rigid or fixed-lever arm systems, and thus fail to capture the dynamic changes in effective lever arm length inherent in a variable geometry design. To address this gap, we developed a kinematic model to describe how the actuator input T_{actuator} and cable-driven transmission translate into assistive torque T_{exo} at the shoulder joint. Specifically, we derived analytical expressions that link the shoulder elevation angle, cable displacement, and resulting moment arm length, enabling precise prediction of assistive torque across the entire range of motion.

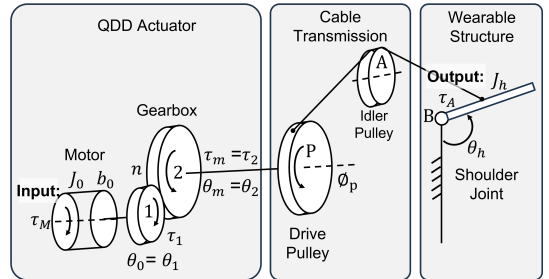


Fig. 7. Human-exoskeleton dynamics model of the shoulder exoskeleton with C-QDD actuation, illustrating the relationship between input motor torque τ_M and output assistive torque τ_A . The system consists of three main modules: the QDD actuator, composed of a high-torque motor with a 6:1 gear ratio planetary gearbox, the cable-driven transmission, and the wearable structure coupled to the human body. The output dynamics are influenced by the wearable structure with inertia J_h and shoulder joint angle θ_h .

To begin with, the actuator produces tension in the cable F_{cable} given by

$$F_{\text{cable}} = \frac{T_{\text{actuator}}}{r_p} \quad (1)$$

where r_p indicates the radius of the drive pulley and $T_{\text{actuator}} = NT_m$ the actuator torque, with T_m being the motor torque and N the gear ratio. In static conditions, the cable tension, in turn, generates assistive torque T_{exo} at the shoulder joint according to the equation

$$T_{\text{exo}} = F_{\text{cable}}l = \frac{T_{\text{actuator}}}{r_p}l \quad (2)$$

where l is the moment arm of the assistive torque.

Considering a simple revolute joint where the cable wraps around a circular pulley, like in the design in [16], the moment arm l is constant and coincides with the radius of the pulley at the shoulder. Consequently, the ratio between the output assistive torque and the input actuator torque is fixed and equal to

$$\frac{T_{\text{exo}}}{T_{\text{actuator}}} = \frac{r_s}{r_p} \quad (3)$$

where r_s is the radius of the pulley at shoulder. Therefore, with this design, a large pulley is required at the shoulder to maximize the torque amplification factor. However, such

a solution is not desirable in terms of added weight and bulkiness near the joint.

In our design, the shoulder joint instead consists of a mechanism where the cable does not wrap directly around the center of rotation, as illustrated in Fig. 4. The mechanism is composed of two links interconnected at the joint B , while the cable wraps around the pulley A and has one end connected to C . This design causes the moment arm (i.e., the distance between the cable and the center of rotation B) to change with the joint angle, that is $l = l(\theta_h)$. Specifically, this relationship is illustrated in Fig. 4c, which indicates that the moment arm increases with the angle in the desired assistance domain, so that stronger assistance is provided as the arm moves toward higher angles, up to 76 mm at about 150°. The analysis of the joint mechanism can be split into two operation areas: small elevation angles (<19°, area in blue in Fig. 4c, and >19°, larger angles (area in orange).

1) Model of Assistive Torque Moment Arm at Small Elevation Angles of Shoulder Joint: For small arm elevation angles (Fig. 4a), the cable wraps around the pulley in B . Thus, the moment arm l coincides with the radius r_B of that pulley.

$$l(\theta_h) = r_B, \quad \text{for } \theta \leq \theta_h^* \quad (4)$$

This relationship holds until the cable remains in contact with the pulley in B , where θ_h^* denotes the critical angle. Theoretically, the critical configuration occurs when the cable is tangent at one point to the pulley in B , i.e., when the trait BC of the cable (with orientation θ_{cBC}) is collinear to the trait AB (with orientation θ_{cAB}). This can be represented by,

$$\theta_{cAB} = \theta_{cBC}, \quad (5)$$

where, from geometrical considerations,

$$\theta_{cAB} = \theta_{AB} - \arcsin\left(\frac{r_A - r_B}{d_{AB}}\right) \quad (6)$$

$$\theta_{cBC} = \theta_{BC} + \arcsin\left(\frac{r_C - r_B}{d_{BC}}\right) \quad (7)$$

In the above equations, d_{ij} and θ_{ij} indicate the distance and the orientation of the segment between the points i and j , while R_i denotes the radius of the pulley centered in i , holding $r_A > r_C > r_B$. Note that all the quantities are constant except for θ_{BC} , which is related to the elevation angle θ_h by a fixed offset $\bar{\theta} = 33.5^\circ$, as defined by the geometry of the distal link:

$$\theta_{BC} = \theta_h + \bar{\theta}. \quad (8)$$

Putting everything together, it yields

$$\theta_h^* = \theta_{AB} - \arcsin\left(\frac{r_A - r_B}{d_{AB}}\right) - \arcsin\left(\frac{r_C - r_B}{d_{BC}}\right) - \bar{\theta} \quad (9)$$

Through our design, by setting the appropriate values of r_A, r_B, r_C , as well as d_{AB}, d_{BC} , we have the critical angle $\theta_h^* = 19^\circ$, which is the boundary angle between the transition from natural upper limb swing to the shoulder elevation.

2) Model of Assistive Torque Moment Arm at Large Elevation Angles of Shoulder Joint: For larger angles (Fig. 4c), the cable does not touch the pulley in B , and the moment arm l substantially increases as the cable moves further from the pulley. From geometrical considerations, the moment arm l is the altitude of the triangle MBN and is computed as

$$l(\theta_h) = \frac{2}{d_{MN}} \sqrt{p(p - d_{MB})(p - d_{BN})(p - d_{MN})}, \quad (10)$$

for $\theta > \theta_h^*$

where p is the semi-perimeter of the triangle MBN

$$p = \frac{1}{2}(d_{MB} + d_{BN} + d_{MN}) \quad (11)$$

Further details on the calculation of the distances d_{MB}, d_{BN}, d_{NM} are reported as follows.

Considering the triangle MBN in Fig. 4b, it can be seen that the moment arm l coincides with the altitude of the triangle orthogonal to MN , i.e., the direction of the cable. The altitude, in turn, is calculated from the distances d_{MB}, d_{BN} , and d_{MN} . Their values can be obtained from the law of cosines as follows:

$$d_{MB} = \sqrt{d_{AB}^2 + r_A^2 - 2d_{AB}r_A \cos(\widehat{MAB})} \quad (12)$$

$$d_{BN} = \sqrt{d_{BC}^2 + r_C^2 - 2d_{BC}r_C \cos(\widehat{NCB})} \quad (13)$$

$$d_{MN} = \sqrt{d_{MB}^2 + d_{BN}^2 - 2d_{MB}d_{BN} \cos(\widehat{MBN})} \quad (14)$$

where the angles $\widehat{MAB}, \widehat{NCB}, \widehat{MBN}$ are

$$\widehat{MAB} = 90^\circ + \alpha - \delta \quad (15)$$

$$\widehat{NCB} = 90^\circ - \gamma + \delta \quad (16)$$

$$\widehat{MBN} = \beta - \widehat{MBA} - \widehat{NBC} \quad (17)$$

and geometrical considerations yield:

$$\beta = 180^\circ + \theta_{AB} - \theta_{BC} \quad (18)$$

$$d_{AC} = \sqrt{d_{AB}^2 + d_{BC}^2 - 2d_{AB}d_{BC} \cos(\beta)} \quad (19)$$

$$\delta = \arcsin\left(\frac{r_A - r_C}{d_{AC}}\right) \quad (20)$$

$$\alpha = \arcsin\left(d_{BC} \frac{\sin(\beta)}{d_{AC}}\right) \quad (21)$$

$$\gamma = \theta_{BC} - \theta_{AC} = \theta_{BC} - \theta_{AB} - \alpha \quad (22)$$

$$\widehat{MBA} = \arcsin\left(r_A \frac{\sin(\widehat{MAB})}{d_{MB}}\right) \quad (23)$$

$$\widehat{NBC} = \arcsin\left(r_C \frac{\sin(\widehat{NCB})}{d_{BN}}\right) \quad (24)$$

Note that θ_{AB}, d_{AB} , and d_{BC} are fixed quantities, determined by the geometry of the mechanism.

B. State-Space Model of Human-Exoskeleton Dynamics for Input-Output Characterization

There is no existing state-space model for shoulder exoskeleton with C-QDD actuation that provides a representation of actuator dynamics, cable transmission characteristics. This section presents a bottom-up derivation of the state-space model for a Cable-Driven Quasi Direct Drive (C-QDD) shoulder exoskeleton with motor voltage as the input and assistive torque as the output. Our state-space model considers both the exoskeleton and human arm dynamics, incorporating the nonlinearities caused by the variable assistive lever arm, the gravitational torque acting on the human arm, as well as the frictions and elastic deformations of Bowden cable transmission. Note that control is not the focus of this work. Our goal is to understand the coupled nonlinear dynamics of human-exoskeleton system and theoretically characterize the relationship between system input and output. This model also provides a foundation for future model-based impedance controllers for the first time.

The C-QDD shoulder exoskeleton system consists of three primary components (Fig. 7): the QDD actuator, the cable transmission mechanism, and the upper arm brace. The actuation comprises a brushless DC electric motor connected to a gear reducer, which transmits force through a drive pulley to the Bowden cable in order to assist upper limb movements.

1) Actuator Dynamics: As an electromechanical system, the actuator dynamics are determined by the interaction of electrical and mechanical quantities.

The electrical behavior of the motor is governed by Kirchhoff's Voltage Law, which relates the input voltage to the motor's internal resistance, inductance, and back electromotive force (EMF). The fundamental equation is:

$$V = Ri + L \frac{di}{dt} + K_e \omega_m \quad (25)$$

where

- V is the input voltage,
- R is the motor's electrical resistance,
- i is the motor current,
- L is the motor's inductance,
- K_e is the back electromotive force constant,
- ω_m is the motor's angular velocity.

Eq. 25 can be rearranged to express the rate of change of current, which is directly related to the motor output torque:

$$\frac{di}{dt} = \frac{1}{L} (V - Ri - K_e \omega_m) \quad (26)$$

The mechanical behavior involves the balance of torques acting on the motor shaft:

$$T_m - T_{\text{load}} = J_{\text{total}} \frac{d\omega_m}{dt} + B_{\text{total}} \omega_m \quad (27)$$

where:

- T_m is the motor torque,
- T_{load} is the load torque,
- J_{total} is the total reflected inertia,
- B_{total} is the total damping coefficient.

The motor torque T_m is generated by the current and is given by

$$T_m = K_t i \quad (28)$$

where K_t is the motor torque constant.

The total reflected inertia and damping are expressed as:

$$J_{\text{total}} = J_m + J_{\text{gear}}^{\text{reflected}} + J_{\text{pulley}}^{\text{reflected}} \quad (29)$$

$$B_{\text{total}} = B_m + B_{\text{gear}}^{\text{reflected}} + B_{\text{pulley}}^{\text{reflected}} \quad (30)$$

where:

- J_m and B_m are the motor's inertia and damping,
- $J_{\text{gear}}^{\text{reflected}} = J_{g1} + \frac{J_{g2}}{N^2}$ and $B_{\text{gear}}^{\text{reflected}} = B_{g1} + \frac{B_{g2}}{N^2}$ represent the reflected inertia and damping of the gear reducer,
- $J_{\text{pulley}}^{\text{reflected}} = \frac{J_p}{N^2}$ and $B_{\text{pulley}}^{\text{reflected}} = \frac{B_p}{N^2}$ are the pulley's inertia and damping,
- N is the inverse of the reducer gear ratio (1:6).

The load torque T_{load} is equal to the assistive torque transmitted to the exoskeleton's shoulder joint T_{exo} scaled down by the gear ratio N :

$$T_{\text{load}} = N \cdot T_{\text{exo}} \quad (31)$$

where the assistive torque T_{exo} can be expressed in turn as a function of the force in the Bowden cable F_{cable} and the variable moment arm $l(\theta_h)$, dependent on shoulder angle θ_h :

$$T_{\text{exo}} = F_{\text{cable}} \cdot l(\theta_h) \quad (32)$$

Thus, substituting T_{load} back into the torque balance equation:

$$T_m - N \cdot F_{\text{cable}} \cdot l(\theta_h) = J_{\text{total}} \frac{d\omega_m}{dt} + B_{\text{total}} \omega_m \quad (33)$$

Solving for $\frac{d\omega_m}{dt}$:

$$\frac{d\omega_m}{dt} = \frac{1}{J_{\text{total}}} (T_m - N \cdot F_{\text{cable}} \cdot l(\theta_h) - B_{\text{total}} \omega_m) \quad (34)$$

2) Bowden Cable Transmission Dynamics Incorporating Changes Between Cable's Distal and Proximal Ends: The Bowden cables transmit force from the actuator to the upper arm wearable structures, converting motor torque into assistive torque at the shoulder joint. The Bowden cable runs from and wraps around a pulley fastened to the QDD actuator's output shaft and goes to the shoulder joint mechanism, where it passes through pulley A, pulley B (hinge), and is fixed to pulley C, as illustrated in Fig. 4. As the motor rotates, it winds or unwinds the cable around the pulley, creating tension that translates into a lifting moment around the hinge B, thereby assisting shoulder motion. The force F_{cable} in the cable is modeled considering both stiffness and damping:

$$F_{\text{cable}} = k_c \Delta x + b_c \Delta v \quad (35)$$

where:

- k_c is the cable stiffness,
- b_c is the cable damping coefficient,

- Δx is the relative displacement between the cable's distal and proximal ends.
- Δv is the relative velocity between the cable attachment points on the drive pulley and the arm brace.

Considering the pulley radius r_p , gear ratio N , and the variable moment arm $l(\theta_h)$, the relative displacement and velocity can be written as:

$$\Delta x = r_p N \theta_m - l(\theta_h) \theta_h \quad (36)$$

$$\Delta v = r_p N \omega_m - l(\theta_h) \omega_h \quad (37)$$

Substituting these into the force equation (Eq. 34):

$$F_{\text{cable}} = k_c (r_p N \theta_m - l(\theta_h) \theta_h) + b_c (r_p N \omega_m - l(\theta_h) \omega_h) \quad (38)$$

where:

- θ_m is the motor's angular position,
- θ_h is the human arm's angular position,
- ω_h is the human arm's angular velocity.

3) *Dynamics of Human Shoulder During Lifting Incorporating Nonlinearity of Gravity Torque:* The human arm is modeled as a rigid body with inherent inertia and damping, interacting with the exoskeleton through assistive torque T_{exo} . The torque balance on the human arm is:

$$T_{\text{exo}} + T_{\text{muscle}} - T_{\text{gravity}}(\theta_h) = J_h \frac{d\omega_h}{dt} + B_h \omega_h \quad (39)$$

where:

- T_{exo} is the assistive torque from the exoskeleton, expressed by Eq. 32
- T_{muscle} is the torque applied by the user muscles, modeled as a disturbance,
- $T_{\text{gravity}}(\theta_h) = m_h g l_h \sin(\theta_h)$ is the gravitational torque of the arm around the shoulder joint, with m_h being the mass of the user's arm, g the gravity acceleration, and l_h the distance between the center of mass of the arm and the axis of the shoulder joint,
- B_h is the human arm's damping coefficient,
- J_h is the human arm's inertia.

Solving for the human arm's angular acceleration:

$$\frac{d\omega_h}{dt} = \frac{1}{J_h} (F_{\text{cable}} \cdot l(\theta_h) + T_{\text{muscle}} - m_h g l_h \sin(\theta_h) - B_h \omega_h) \quad (40)$$

4) *State-Space Modeling of Human-Shoulder Exoskeleton Interaction:* To facilitate analysis and control design, the system is represented in a state-space framework. The state-space equations are derived by consolidating the C-QDD actuation and human arm dynamics based on previous derivations:

$$\dot{\mathbf{x}} = \mathbf{A}(\theta_h)\mathbf{x} + \mathbf{f}(\theta_h) + \mathbf{B}u + \mathbf{D}d \quad (41)$$

$$y = \mathbf{C}\mathbf{x} + \mathbf{E}u + \mathbf{F}d \quad (42)$$

where the state vector \mathbf{x} is defined as:

$$\begin{aligned} \mathbf{x} &\triangleq \begin{bmatrix} x_1 & x_2 & x_3 & x_4 & x_5 \end{bmatrix}^T \\ &= \begin{bmatrix} i & \theta_m & \theta_h & \omega_m & \omega_h \end{bmatrix}^T \end{aligned} \quad (43)$$

and:

- $y = T_{\text{exo}}$ is the output (assistive torque),
- $u = V$ is the control input (motor input voltage).
- $d = T_{\text{muscle}}$ is the disturbance input (user muscle effort).

The matrices $\mathbf{A}(\theta_h)$, $\mathbf{f}(\theta_h)$, \mathbf{B} , \mathbf{C} , \mathbf{D} , \mathbf{E} , and \mathbf{F} are defined as:

$$\begin{aligned} \mathbf{A}(\theta_h) &\triangleq \\ &\triangleq \begin{bmatrix} -\frac{R}{L} & 0 & 0 & -\frac{K_e}{L} & 0 \\ 0 & 0 & 0 & 1 & 0 \\ 0 & 0 & 0 & 0 & 1 \\ \frac{K_t}{J_{\text{total}}} & -\frac{k_c r_p N^2 l(\theta_h)}{J_{\text{total}}} & \frac{k_c N l^2(\theta_h)}{J_{\text{total}}} & a_{44}(\theta_h) & \frac{b_c N l^2(\theta_h)}{J_{\text{total}}} \\ 0 & \frac{k_c r_p N l(\theta_h)}{J_h} & -\frac{k_c l^2(\theta_h)}{J_h} & \frac{b_c r_p N l(\theta_h)}{J_h} & a_{55}(\theta_h) \end{bmatrix} \\ a_{44}(\theta_h) &= -\frac{b_c r_p N^2 l(\theta_h) + B_{\text{total}}}{J_{\text{total}}} \\ a_{55}(\theta_h) &= -\frac{b_c l^2(\theta_h) + B_h}{J_h} \\ \mathbf{f}(\theta_h) &\triangleq \begin{bmatrix} 0 & 0 & 0 & 0 & -\frac{m_h g l_h}{J_h} \sin(\theta_h) \end{bmatrix}^T \\ \mathbf{B} &\triangleq \begin{bmatrix} \frac{1}{L} & 0 & 0 & 0 & 0 \end{bmatrix}^T, \quad \mathbf{D} \triangleq \begin{bmatrix} 0 & 0 & 0 & 0 & \frac{1}{J_h} \end{bmatrix}^T \\ \mathbf{C} &\triangleq \begin{bmatrix} 0 & k_c r_p N l(\theta_h) & -k_c l^2(\theta_h) & b_c r_p N l(\theta_h) & -b_c l^2(\theta_h) \end{bmatrix} \\ \mathbf{E} &\triangleq \mathbf{0}, \quad \mathbf{F} \triangleq \mathbf{0} \end{aligned}$$

The dynamic modeling of the human-exoskeleton interaction provides insights into the operational characteristics of the device and lays a foundation for analyzing and optimizing the overall performance, ensuring that it meets the desired criteria of high torque density.

The total reflected inertia J_{total} is a critical factor in achieving a lightweight system. With the low gear ratio planetary gear QDD actuation, the overall system inertia can be significantly reduced. A lower J_{total} enhances the system's responsiveness, allowing for swift acceleration and deceleration without adding excessive weight. Additionally, employing lightweight materials in the construction of the motor, gear reducer, and pulleys further contributes to minimizing the device's mass, ensuring ease of use and reducing fatigue for the user.

The assistive torque T_{exo} is directly proportional to the force exerted by the Bowden cable F_{cable} , and in turn to the motor torque constant K_t and the gear ratio N . Therefore, the high torque constant K_t and low gear ratio N of QDD actuation, combined with the low friction loss of the Bowden cable transmission, enable the C-QDD-based shoulder exoskeleton to generate high torque outputs necessary for assisting a wide range of shoulder movements while maintaining a lightweight design.

C. Biomechanical Model of the Shoulder Biological Torque for Gravity Compensation Control Strategy

Despite controller design is not the focus of this study, we chose to develop a simple but effective gravity compensation strategy, where the exoskeleton assistance aims to support the biological torque by compensating for the effect of gravity on the arm. In the case of partial assistance, the desired assistive torque T_{desired} is assumed equal to a fraction K of the gravitational torque acting on the shoulder T_{gravity} :

$$T_{\text{desired}} = KT_{\text{gravity}} = Km_h g l_h \sin(\theta_h), \quad (44)$$

In general, the distance l_h varies with the posture of the arm. For simplicity, here we consider the scenario that needs the highest torque support, corresponding to the arm in the fully extended configuration. Furthermore, the quantities m_h and l_h can be expressed as functions of user body weight w_{user} and height h_{user} using relative proportions from anthropometric studies [43], in the form

$$m_h = C^w w_{\text{user}} \quad (45)$$

$$l_h = C^G l_{\text{arm}} = C^G C^h h_{\text{user}} \quad (46)$$

As a result, the gravity torque T_{gravity} can be estimated as

$$T_{\text{gravity}} = C^w C^G C^h h_{\text{user}} w_{\text{user}} g \sin(\theta_h), \quad (47)$$

where the above-mentioned coefficients are reported in Table III and their derivation is detailed as follows.

Anthropometric studies allow the expression of the anatomical data of single body segments as proportions of body weight and height. With respect to the upper limbs, Table III reports the anthropometric parameters of the upper arm, forearm, and hand, where C^w , C^h , and C^G indicate, respectively, the segment weight as a percentage of total body weight, the segment length as a percentage of total height, and the location of the segment center of gravity as a percentage of the segment length [43].

TABLE III
ANTHROPOMETRIC PARAMETERS FOR BIOLOGICAL TORQUE ESTIMATION.

	male			female		
	C^w	C^h	C^G	C^w	C^h	C^G
Upper arm (U)	3.25	17.2	43.6	2.9	17.3	45.8
Forearm (F)	1.87	15.7	43.0	1.57	16.0	43.4
Hand (H)	0.65	5.75	46.8	0.5	5.75	46.8
Whole arm	5.77	38.65	41.39	4.97	39.05	40.72

Therefore, for the whole arm,

$$\begin{aligned} m_h &= m_U + m_F + m_H \\ &= w_{\text{user}}(C_U^w + C_F^w + C_H^w). \end{aligned} \quad (48)$$

Hence,

$$C^w = C_U^w + C_F^w + C_H^w. \quad (49)$$

Further, considering the arm in its fully extended configuration, yields

$$\begin{aligned} l_{\text{arm}} &= l_U + l_F + l_H \\ &= h_{\text{user}}(C_U^h + C_F^h + C_H^h), \end{aligned} \quad (50)$$

namely,

$$C^h = C_U^h + C_F^h + C_H^h, \quad (51)$$

While C^G is the weighted sum of the single contributions, that is

$$\begin{aligned} C^G = &\frac{1}{C^w C^h} [(C_U^G C_U^h) C_U^w + (C_U^h + C_F^G C_F^h) C_F^w + \\ &+ (C_U^h + C_F^h + C_H^G C_H^h) C_H^w]. \end{aligned} \quad (52)$$

Therefore, putting all together, given the desired torque at the shoulder T_{desired} , and taking into account the transmission efficiency η_T , the torque required by the actuator T_{actuator} can be computed as

$$\begin{aligned} T_{\text{actuator}} &= \frac{r_p}{l(\theta_h) \eta_T} T_{\text{desired}} \\ &= \frac{r_p}{l(\theta_h) \eta_T} \frac{K}{C^w C^G C^h} h_{\text{user}} w_{\text{user}} g \sin(\theta_h) \end{aligned} \quad (53)$$

VII. GRAVITY COMPENSATION CONTROL OF SHOULDER EXOSKELETON

Shoulder exoskeletons must counteract the gravitational torque that increases nonlinearly with arm elevation, requiring an intuitive controller that continuously delivers appropriate assistance based on the user's motion and desired support level, without relying on excessive input. *Although control is not the focus of this work, we developed a gravity-compensation controller that scales assistive torque in proportion to the user's shoulder elevation.* To provide appropriate assistance in dynamic tasks where the elevation of the arms changes along with the human shoulder lifting angle over time, the robots need to estimate the user arm kinematics. In this work, we deployed one IMU sensor (Alubi LPMS-B2) that is placed on each upper arm to measure the movements of the upper arm. The arm elevation angle is estimated from the angles provided by the internal Kalman filter of the IMUs. A quick static calibration of the IMUs is performed on startup to reset the IMU's readings while the user is in their neutral position, with arms down along the torso. The robot controller then maps the shoulder elevation angle θ_h to the assistive torque T_{exo} using the biomechanical model and cable transmission model described in Sec. VI.

The control framework of the exoskeleton is illustrated in Fig. 8, which presents a two-layer architecture with high-level and low-level control modules. The high-level control uses the kinematic information from the IMUs to determine the desired assistive torque at the shoulder and the reference torque for the actuator via the exoskeleton's transmission, while the low-level control framework maps the reference torque to the motor current through the motor torque constant. A gravity compensation controller was designed to offload the wearer's limb from the effects of gravity, with the level of assistance as an input parameter. The gravity compensation controller uses the pose of the limb and user-specific anthropometric data (height and weight) to compute a desired torque profile, which is, in turn, tracked by the low-level controller. Once the user initiates the motion, the robot reacts in real-time, and the amount of support is adjusted based on the elevation angle of the user's arm. A minimum shoulder elevation threshold for

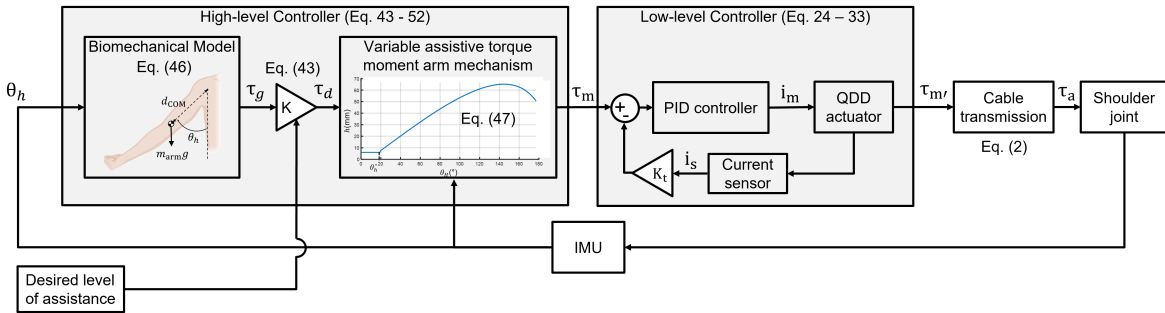


Fig. 8. Schematic of the gravity compensation control system. The robot uses anthropometric data (user's body weight and height) and shoulder joint angle detected by the IMU sensor to estimate (Eq. 46) the biological torque required to sustain the arms against gravity. An additional parameter allows the user to set desired level of assistance as a percentage of the estimated gravitational torque (Eq. 43). The torque required by the actuator can be calculated by substituting the desired torque at shoulder joint into the cable transmission model (Eq. 47). The closed-loop low-level PID controller ensures accurate tracking of the torque command with collocated current sensors embedded on the actuator driver.

support was implemented to avoid unexpected torque assistance at very small elevation angles. The nonlinear mapping of upper limb lifting angle to actuator torque was adjusted to each user based on anthropometric data. For the human experiments, the exoskeleton was set to provide the user with an assistive torque T_{exo} that corresponded to 50% of the torque T_{gravity} required to balance their arm against gravity. The motor then generated the mechanical power required to assist the shoulder, thereby closing the outer torque control loop.

VIII. EXPERIMENTS AND RESULTS

To evaluate the performance of the shoulder exoskeleton, we conducted both benchtop and human subject experiments. The benchtop experiments aimed to verify the design methods of the variable lever arm mechanism and evaluate the performance of the high torque density cable-driven quasi-direct drive actuation, and characterize the relationship between the motor current input and assistive torque out, at different shoulder lifting angles. The human experiment shows that our shoulder exoskeleton can provide effective torque assistance and significantly reduce human muscle effort for both overhead work and lifting, and muscle fatigue.

A. Benchtop Evaluation of Shoulder Exoskeleton Mechatronic Performance with Variable Lever Arm Mechanism and Cable-QDD Actuation

The mechanical characterization tests were comprised of assistive torque T_{exo} assessments at different elevation angles θ_h and under varying motor torque inputs, whereby the motor torque T_m is directly proportional to the motor current i through the torque constant K_t , governed by Eq. 28. A force sensor was used to measure the force F normal to the arm support at a distance d from the joint axis, resulting in the output torque T_{exo} , as shown in Fig. 9a. Angles ranged between 15° and 150° at a step of 15°. Each measurement was taken 3 times per condition and data averages and standard deviations were calculated. As expected, the results in Fig. 9b indicate that the joint torque T_{exo} is linearly proportional to the motor current (and thus to the motor torque), and the slope increases with the elevation angle. This is confirmed by Fig. 9c, which shows that at constant motor current the joint torque increases with the elevation angle and their relationship reflects the variation of the moment arm due to the cable transmission

design, as presented in Sec. VI. The maximum assistive torque of approximately 11 Nm was recorded at 150° elevation angle when a current of 10 A was commanded to the motor.

B. Shoulder Joint Range-of-Motion Changes to Evaluate the Effect of Variable Lever Arm Mechanism to Mitigate Physical Interference Between Robot and Natural Shoulder Movement

TABLE IV
MERGE THIS TABLE WITH THE EMG RESULT ONE BENCHMARK COMPARISON: LOWEST REDUCTION IN SHOULDER RANGE OF MOTION COMPARED TO NO EXOSKELETON CONDITION

Research	Reduction in Range of Motion Compared to No Exo Condition
This work	< 8%
ETH [17] NMI 2022	22.7%
UT Austin [23] IJRR 2017	> 30% in abduction
Sant'Anna [22] ICORR 2019	> 31% in flexion > 60% in abduction
Sant'Anna [49] RAM 2020	23% in abduction

Arm movements in activities of daily living typically fall in the range 20° to 120° of shoulder elevation angle [48], [50]–[52]. For the evaluation of the range of motion, participants were asked to lift their arms to their maximum extent in four vertical planes with angular displacements of 0°, 45°, 90°, and 135° with respect to the frontal plane. To prevent ballistic trajectories of the arm, participants were instructed to hold their maximum elevation for 2 seconds. Experimental measurements (Fig. 11) showed that the maximal humeral elevation with the device unpowered was slightly lower ($134.9^\circ \pm 13.3^\circ$) compared to movements without the device ($145.5^\circ \pm 13.7^\circ$), corresponding to a 7.3% average reduction of the range of motion. Nonetheless, the elevation requirements for most activities of daily living fall within the achieved range of motion, which means that the exoskeleton allows users to perform natural movements, selectively assisting shoulder elevation without over-constraining horizontal flexion or extension. These results suggest that the exoskeleton design minimizes mechanical interference with the user, ensuring the device adapts seamlessly to the user's natural biomechanics during functional tasks.

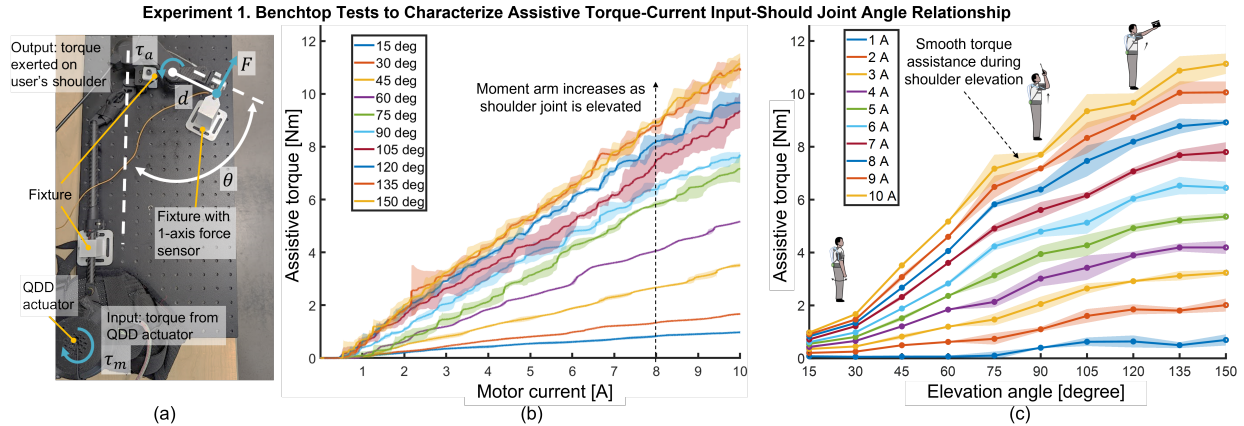


Fig. 9. Benchtop validation of the C-QDD shoulder exoskeleton confirms smooth, linear torque assistance and the effectiveness of the variable lever arm mechanism. (a) Experimental setup for measuring assistive torque as a function of motor current (Eq. 27) and simulated shoulder elevation angle (Eq. 2). (b) Measured assistive torque is linearly proportional to the motor current input, with the slope increasing at higher elevation angles. (c) At larger elevation angles, the system produces higher torque for the same current input, validating the variable lever arm design and the theoretical predictions (Eq. 9). The torque-current relationship maintains good linearity across the elevation range without mechanical dead points. The maximum current was limited to below 10 A for safety, though the actuator supports peak currents up to 13 A.

Order of these tests was randomized									
Condition	Baseline (no exoskeleton) / Exoskeleton assist on							Rest	No exoskeleton
Test	Active range of motion	Rest	Set up sEMG sensors	Rest	Simulated ADLs	Rest	Static hold assessment	Rest	System usability scale, Borg scale
Duration time	3 min	3 min	45 min	3 min	15 min	15 min	Until feel fatigue	15 min	10 min
Instruments	Inertial measurement unit (IMUs)	Timer	sEMG sensor	Timer	Inertial measurement unit (IMUs), sEMG sensors	Timer	Timer, Inertial measurement unit (IMUs), sEMG sensors	Timer	-
Metrics	Shoulder elevation angle (°)	-	N.A.	-	Shoulder elevation angle (°), Muscle activations	-	Duration time, Shoulder elevation angle (°), Muscle activations	-	Usability score, Borg score
Purpose	To validate method 1.2 to mitigate physical interference		To capture sEMG signals		To validate method 2 lightweight C-QDD actuation		To validate method 1.1 to enable assistance without joint misalignment		

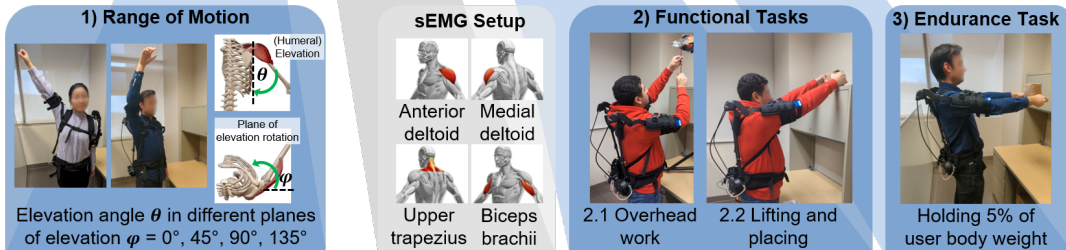


Fig. 10. Experimental protocol for human testing ($n=7$, non-disabled) evaluating the physical interference and assistance effectiveness of the shoulder exoskeleton. We conducted human experiments of overhead work, lifting, and enhancing muscle endurance under two conditions: “no exo” (without device) and “assist on” (powered exoskeleton). Outcome measures were compared with respect to three outcome metrics: active range of motion, muscular activity during functional tasks, and endurance time. sEMG electrodes and sensors were placed after the active range of motion test to eliminate the potential influence on the range of motions caused by the sensors and their wrappings. The two functional tasks, i.e., overhead work and lifting and placing, and the endurance tasks are conducted in randomized crossover trials. Subjective feedback from the participants on the perceived exertion and usability of the device was collected at the end of the experiments.

C. Human Evaluation on Assitance Effect of Shoulder Exoskeleton with Biomimetic Mechanism Design and Cable-QDD Actuation

The human experiments aimed to evaluate the device's effectiveness in assisting shoulder elevation during functional tasks. The impact of the exoskeleton was assessed based on three relevant outcome metrics: range of motion, muscular activity, and endurance. Seven non-disabled participants were enrolled in the experiment (age 29.7 ± 2.3 years, body weight 77.6 ± 14.7 kg, and height 1.74 ± 0.09 m). Inclusion criteria include anthropometric sizes of the participants within the ranges accommodated by the device, no evidence or known history of musculoskeletal or neurological diseases, and nor-

mal joint range of motion and muscle strength. All subjects were informed of the experiment protocol and provided explicit written consent before participating in the study. Our experiment protocol was approved by the Institutional Review Board under Application No. eIRB #25147.

The experiment protocol is shown in Fig. 10. Before the initiation of the experiment, a familiarization phase allowed the participants to experience the assistance and acclimate to the device. Then, various tests were performed to evaluate the effect of the exoskeleton on the range of motion, muscular activity during two functional tasks, and endurance. For each test, the level of assistance was set to 50% of the biological torque, and the order of testing conditions (with

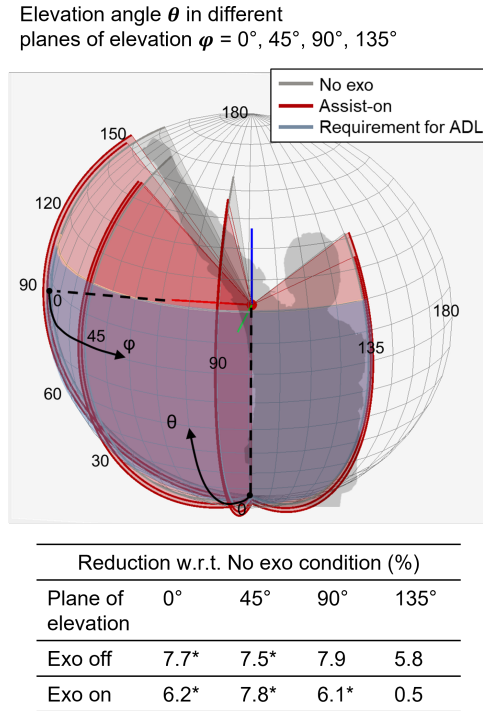


Fig. 11. Range-of-motion results ($n=7$) show that our variable lever arm mechanism minimizes physical interference between the exoskeleton and the user's shoulder, with only a minimal reduction of the range of motion (less than 8%). In contrast, most state-of-the-art robots can result in more than 30% reduction of range of motion [13], [22]. Additionally, the maximum range of motion in arm elevation required to perform most daily activities [48] is still fulfilled when the shoulder exoskeleton is used. Significant differences per the paired-sample t-test are indicated with * for $p\text{-value} < 0.05$.

and without exo) was randomized. Surface electromyography (EMG) signals were used as a metric to quantify the effort that the user required for the musculoskeletal system. We recorded the muscle activity of 4 muscles (right arm): medial deltoid (MD), anterior deltoid (AD), upper trapezius (UT), and biceps brachii (BB). Electrodes were placed according to the SENIAM guidelines [53], ensuring that they were not colliding with the straps or the cuff of the device. Before starting the experiments, we collected maximum voluntary contraction (MVC) of the recorded muscles. The MVC was used to normalize all the other EMG data in postprocessing, to allow for intra-subject comparison. Raw EMG signals were acquired at 2 kHz with the proprietary software of the wireless surface EMG system, Noraxon Ultium (Noraxon, USA). The raw sEMG signals were smoothed using a root mean square (RMS) algorithm with a window size of 100 ms and then normalized to each participant's MVC. At the end of the experiments, participants provided a subjective evaluation of the perceived effort during the activities using the Borg rating of perceived exertion and of the overall comfort and usability of the device through a 5-score Likert scale questionnaire. For statistical analysis, task performance with and without exoskeleton was compared using a paired-sample T-test. The significance level was set at a $p\text{-value}$ of 0.05.

1) Shoulder Muscles Activity Reduction During Functional Tasks: Two dynamic tasks were performed to evaluate the effectiveness of the device during functional activities. Task 1 consisted of an overhead assembly task, where the subject

had to tighten four screws using a screwdriver, while task 2 involved lifting an object (5% user body weight) from the table (height 74 cm) and placing it to a target location on a shelf (height 165 cm), performing 3 repetitions. The user's muscular activity was compared across the conditions without exoskeleton (No-exo) and with device assistance (Assist-on).

For the overhead assembly task, the analysis involved only the time for completing the screwing operation itself, excluding the phases of raising and lowering the arms, while for the lift and place test, the muscle activation during the object lifting phase was considered. Fig. 12 and Fig. 13 show the average muscle activity during the two functional tasks. For all the recorded muscles, muscle activity was less pronounced with exoskeleton assistance compared to the baseline condition. Specifically, EMG reduction was especially significant for the anterior deltoid and medial deltoid, which have a primary role in shoulder flexion/extension and abduction/adduction, respectively. These results apply to both the overhead work task (Fig. 12), where average reductions of 52.8% and 65.2% were recorded for anterior deltoid and medial deltoid, respectively, and to the lift and place task, as confirmed by the activation profiles in Fig. 13. The bio-inspired design to enable misalignment compensation and 2-DOF assistance was also proven effective in reducing EMG activity in the anterior and medial deltoids during the functional tasks, considering the versatile shoulder lifting angles among different users. This highlights the design's ability to adapt to varied shoulder movements for versatile tasks in different real-world applications.

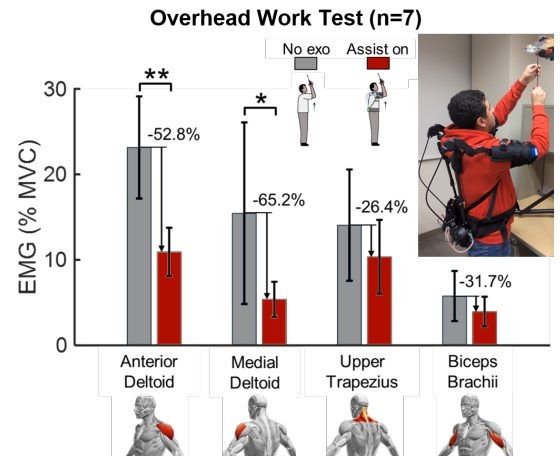


Fig. 12. Overhead work results show significant reductions in muscle activation with exoskeleton assistance. Average sEMG activity decreased by 52.8% (anterior deltoid), 65.2% (medial deltoid), 26.4% (upper trapezius), and 31.7% (biceps brachii), showing effective muscular offloading during the pick-and-place task. Statistical significance from paired-sample t-tests is indicated (* for $p\text{-value} < 0.05$ and ** for $p\text{-value} < 0.01$).

2) Improved Endurance in Payload Holding for Both Shoulder Abduction and Flexion to Validate Effectiveness of Biomimetic Mechanism Design: The final experiment assessed the impact of assistance on muscular endurance, i.e., the maximum amount of time for which a muscle can maintain a certain effort. The endurance was evaluated for the static task of bimanually holding an object (5% user body weight) with arms fully extended forward at 90° elevation in shoulder flexion.

Results are shown in Fig. 14, which indicates that on average

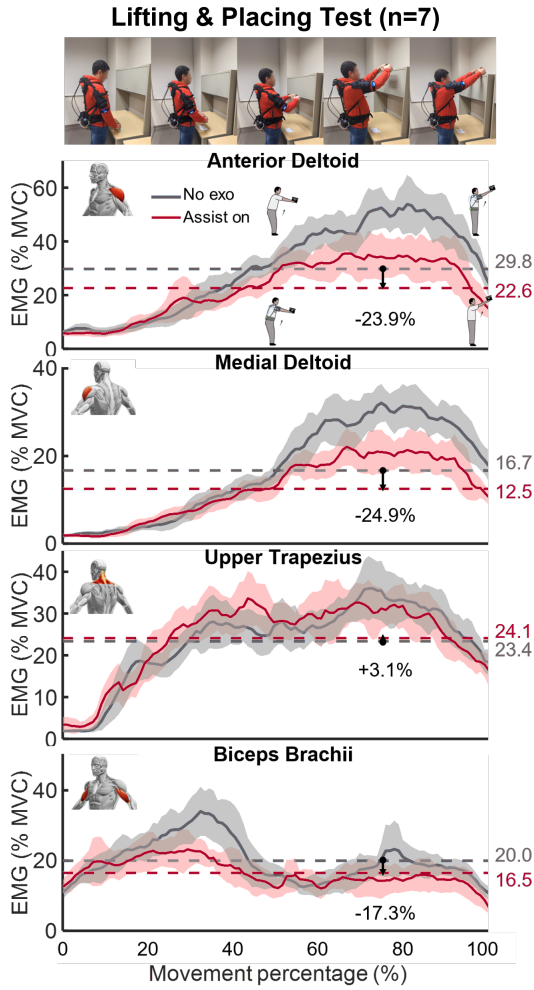


Fig. 13. Lifting-and-placing test results show reduced muscle effort in the deltoid muscles with exoskeleton assistance. Average EMG reductions were 23.9% (anterior deltoid), 24.9% (medial deltoid), and 17.3% (biceps brachii). A slight EMG increase (+3.1%) occurred in the upper trapezius but was minimal compared to overall muscular benefit, confirming effective assistance during the task.

subjects were able to hold the weight for a duration of 73.2% longer when assistance was provided compared to the baseline condition without the device, with the average endurance time increasing from 73 s to 126 s. This result is supported by the fact that on average, the activity of recorded muscles was significantly reduced. Specifically, average EMG reduction due to assistance was 41.5% for the anterior deltoid, 48.7% for the medial deltoid, 30.5% for the upper trapezius, and 44.4% for biceps brachii.

To further extend these results and validate the effectiveness of assistance also for abduction movements, an additional experiment was performed in a subsequent phase of the study. Four subjects underwent a second endurance experiment, where their effort was evaluated for the task of holding a load (3% of user's body weight) with the right arm fully extended to the side at 90° elevation (shoulder abduction). Results are shown in Fig. 14, which indicates that on average subjects were able to hold the weight for a duration of 54.1% longer when assistance was provided compared to the baseline condition without the device, with the average endurance time

increasing from 59 s to 91 s. This result is supported by the fact that on average, the activity of recorded muscles was significantly reduced. Specifically, average EMG reduction due to assistance was 34% for the anterior deltoid, 19% for the medial deltoid. Instead, the activation of the upper trapezius increased on average by 12%.

3) *Positive Subjective Feedback of Comfort and Usability of the Exoskeleton:* At the end of the testing session, participants underwent an overall evaluation survey using the standard system usability scale (SUS) [54] to collect feedback on the overall comfort and usability of the device. SUS score was 76.4, indicating that the exoskeleton has good usability according to the subjects. Participants found it comfortable, easy to don and doff, and they were confident using it throughout the experimental session.

Moreover, the high comfort levels reported through the SUS also indicate that the shoulder exoskeleton felt natural and unobtrusive during use. This feedback aligns with the biomimetic design's goal of reducing perceived exertion by allowing users to retain control over horizontal shoulder movements while providing assistance for tasks that involve lifting against gravity. The ability to balance assistance and natural movement contributed to both subjective comfort and usability, making the exoskeleton more intuitive and user-friendly.

In addition, at the end of each test, we assessed participants' perception of the exercise intensity using the standard Borg Rate of Perceived Exertion (RPE) [55], [56]. All seven participants reported less fatigue with the exoskeleton assistance compared with not wearing the device. For the overhead work task, the average RPE scores (higher value means more fatigue) were 11.4 ± 4.0 and 8.4 ± 2.2 for the no-exo and assisted conditions, respectively. Likewise, for the pick-and-place task, the RPE score decreased from 11.1 ± 3.0 without the robot to 8.7 ± 2.4 when assistance was provided.

IX. DISCUSSION AND CONCLUSION

In this work, we presented the design of a lightweight, compact hybrid soft shoulder exoskeleton with a C-QDD actuation for continuous torque assistance during overhead work, lifting, and endurance tasks. The proposed methods resulted in a portable, compact shoulder exoskeleton with the most lightweight design and the highest torque density among state-of-the-art powered shoulder exoskeletons. Leveraging the bio-inspired design, for each side, the exoskeleton can assist the shoulder flexion and abduction with a C-QDD actuation unit. The contributions of this research are significant for the following reasons. 1) We proposed a self-aligning shoulder exoskeleton that enables assisting a broad range of upper limb movements with minimized physical interference between robot and human shoulder natural movements. 2) We presented the mechatronics design, kinematics modeling, and state-space modeling for a portable shoulder exoskeleton with a C-QDD actuation unit. The presented theory and model delineate the advantages of the proposed C-QDD actuation in comparison with the existing actuation methods, like SEA or pneumatic-sourced actuation. 3) We evaluated and demonstrated a portable shoulder exoskeleton to reduce muscle

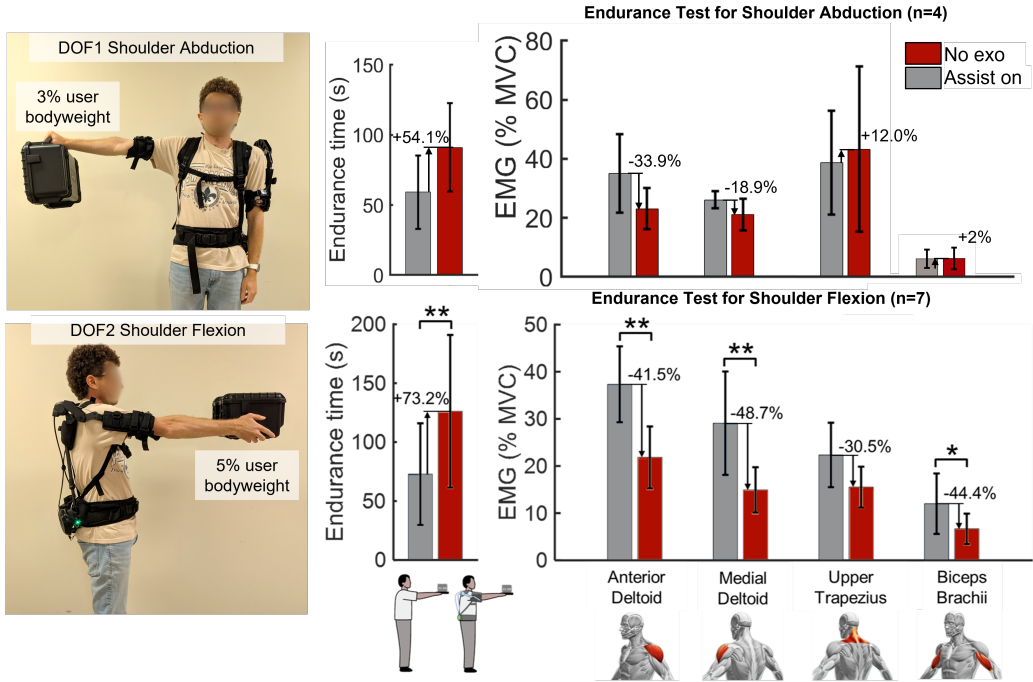


Fig. 14. Endurance test results demonstrate significantly increased holding time and reduced muscle activation with exoskeleton assistance, confirming effective support in both shoulder flexion and abduction enabled by the biomimetic self-aligning mechanism. For flexion, average endurance time increased by 73.2% (from 73 s to 126 s). EMG activity significantly decreased by 41.5% (anterior deltoid), 48.7% (medial deltoid), 30.5% (upper trapezius), and 44.4% (biceps brachii). For abduction, the average muscular endurance time for weight holding significantly increased from 59 s to 91 s (+54.1%) with powered assistance compared to not wearing the device. This result is supported by the fact that, on average, the activity of engaged muscles significantly decreased, with reductions of 34% and 19% for anterior deltoid and medial deltoid muscles, respectively. Statistical significance from paired-sample t-tests is indicated (* for p -value < 0.05 and ** for p -value < 0.01.). Note: An issue with the EMG sensor on the Biceps Brachii was encountered with two subjects during the abduction test, thus their BB EMG was excluded from the analysis.

TABLE V

HUMAN PERFORMANCE COMPARISON: HIGHEST NET REDUCTION IN MUSCLE ACTIVITY AND ENDURANCE IMPROVEMENT

Research	Year	Number of Subjects	Reference Condition	Endurance Time (Exp 3.3)	Mean Muscle Activity Reduction Overhead Work (Exp. 3.1)	Mean Muscle Activity Reduction Lifting and Placing (Exp. 3.2)	Mean Muscle Activity Reduction Holding (Exp. 3.3)
This work	2025	n=7, non-disabled	No exo (net benefit)	+73.2%	AD -52.8%, MD -65.2%, UT -26.4%, BB -31.7%	AD -23.9%, MD -24.9%, UT +3.1%, BB -17.3%	AD -41.5%, MD -48.7%, UT -30.5%, BB -44.4%
NUS [16]	2024	n=10, non-disabled	No exo (net benefit)	N.A.	AD -20.6%, MD -25.4%, UT +6.2%, BB -12.9%, TB +0.1%, LES +0.8%, TM -4.6%	N.A.	N.A.
Harvard [14]	2024	n=9, non-disabled	No exo (net benefit)	N.A.	AD (N.S.) , MD -30%, PD -39%, BB (N.S.), LD (N.S.)	N.A.	AD -29%, MD -43%, PD -43%, BB -49%, LD -32%
ETH [17]	2022	n=8, non-disabled	Assist off (gross benefit)	+36.1%	N.A.	AD -41.8%, MD -3.73%, UT -49.1%, BB -39.7%, LT -32.6%	N.A.
Rossini [57]	2021	n=6, non-disabled	No exo (net benefit)	N.A.	AD -21.5%, UT +3.1%, TB +17.9%	AD -12.9%, UT -7.8%, TB +7.4%	N.A.

Abbreviations: N.A. = Not available, N.S. = Not significant, AD = Anterior Deltoid, MD = Middle Deltoid, PD = Posterior Deltoid, UT = Upper Trapezius, BB = Biceps Brachii, TB = Triceps Brachii, LD = Latissimus Dorsi, LES = Lumbar Erector Spinae, TM = Teres Major. Exp. = Experiment.

activity in non-disabled individuals during simulated activities of daily living, i.e., overhead work, lifting and placing, and static holding.

A. Portable Assistive Shoulder Exoskeleton with C-QDD Actuation: Most Lightweight, Highest Torque Density

Leveraging the C-QDD actuation paradigm, we created the most lightweight powered assistive shoulder exoskeleton. Benchmark and simulated results also demonstrate that the proposed shoulder exoskeleton outperforms state-of-the-art

shoulder exoskeletons by simultaneously meeting the requirements of high torque density and portability. In addition to the actuation system, the hybrid soft exoskeleton design also helps to reduce the weight while ensuring effective torque transmission of the robot. The carbon fiber skeleton that connects the upper limb and the user's waist is also strong enough to transmit the weight from the upper limb to the user's lower back, thus further reducing the weight penalty. To mitigate the physical interference between shoulder exoskeleton and human natural shoulder joint moment, we

designed a variable lever arm mechanism that enables the moment arm of assistive torque to increase as the shoulder is elevated, where higher torque assistance is needed. Compared to some state-of-the-art shoulder exoskeletons that utilize a pulley with a constant radius to provide assistive torque, our design significantly reduces the volume of needed components, therefore minimizing the potential range of motion reduction due to interference between the exoskeleton and the human upper arm. With passive hinges located at the connection part of the rigid frame to the upper arm and waist, respectively, our shoulder exoskeleton enables using one actuator to achieve both shoulder flexion and abduction for each unilateral side of the shoulder joint, thus promoting the design simplicity.

B. Significant Muscles Activation Reduction in All 4 Recorded Upper Limb Muscles

The results of this study demonstrated that the use of the proposed shoulder exoskeleton led to significant reductions in muscle activation during lifting movements and overhead work. Notably, the exoskeleton provided substantial assistance to the anterior and medial deltoid muscles, which are primarily responsible for shoulder flexion and abduction. The reduction in muscle activation was particularly pronounced, with sEMG reductions of 52.8% and 65.2% observed in the anterior and medial deltoids, respectively, during overhead work tasks (Fig. 12). These findings are in line with previous studies on upper-limb exoskeletons that have reported similar reductions in shoulder muscle activity, particularly in the deltoid muscles, which bear the brunt of shoulder lifting [19], [50]. In addition to the deltoids, the results showed a meaningful reduction in the activity of the upper trapezius and biceps brachii muscles during both overhead work and lifting tasks. The upper trapezius, responsible for scapular stabilization and shoulder elevation, exhibited a 26.4% reduction in sEMG activity, while the biceps brachii, which aids in shoulder flexion, saw a 31.7% reduction during overhead work. These reductions, compared to the no-exoskeleton condition, reflect the net benefits of using the exoskeleton.

The capability of the exoskeleton to reduce muscle activity is particularly relevant for tasks requiring prolonged overhead work, which are known to place considerable strain on the shoulder. By offloading the demand on key muscles, the exoskeleton could enhance endurance and reduce fatigue, which makes it a valuable tool for both industrial workers and individuals with upper limb impairments. Additionally, the ability to offload the muscles suggests that the exoskeleton could mitigate the risks of musculoskeletal disorders (MSDs), particularly those related to repetitive shoulder elevation, such as rotator cuff injuries.

C. Limitations and Future Work

Despite these encouraging results, we acknowledge several limitations in our study. First, the assistive torque used in this study was designed to mimic the biological torque, which is an intuitive control approach often employed in wearable robotics. While this method is straightforward, some studies suggest that the optimal exoskeleton torque profile

for enhancing human performance may not necessarily align proportionally with the biological torque [58]. Determining the ideal torque profile remains a complex challenge, as it requires a clear understanding of human–exoskeleton interaction, particularly how assistive torque influences the dynamics of human muscles. However, we chose a proportional biological torque profile because it is a practical, viable solution that is unlikely to negatively affect human performance, making it a solid foundation for providing assistance to wearers. Another limitation of this study is the simplified control strategy, which calculates only the torque needed at the shoulder joint to compensate for the gravitational load of the fully extended arm. Therefore, while the gravitational force usually represents the major portion of the loading, this model does not account for the full dynamics of the entire arm. This simplification may limit the system’s responsiveness in tasks involving rapid accelerations or external disturbances. Future work will explore more advanced control strategies, such as model predictive control or machine learning-based torque estimation, to enable faster response to adjust assistance based on user motion dynamics. Additionally, integrating more comprehensive biomechanical models and additional sensory feedback (e.g., myoelectric signals) could enhance torque estimation accuracy with a better capture of the entire motion of arm and thus more accurately estimate the full shoulder dynamics during various tasks, leading to improved adaptability across a broader range of upper limb tasks.

The second limitation of the experimental study is the focus on non-disabled subjects who have no experience with overhead work, and it is possible that the effects of the exoskeleton may differ from those of experienced workers. Similarly, the results may not fully represent the performance of the exoskeleton in populations with upper limb impairments. While significant reductions in muscle activation were observed, the effects could differ in users with weaker or less coordinated upper limbs. Additionally, the evaluation primarily relied on sEMG reductions, changes in range of motion and user comfort ratings. More comprehensive indicators, such as metabolic cost, joint kinematics, and long-term usability assessments, will be incorporated in future studies to provide a more holistic evaluation of the exoskeleton’s performance. Further testing with impaired users and in real-world scenarios will also be necessary to understand the long-term impact of using the exoskeleton in reducing the risks of shoulder-related musculoskeletal disorders or the improvement in upper limb functional movements for people with shoulder joint mobility impairments, such as people with amyotrophic lateral sclerosis (ALS) [28].

D. Conclusion

In this study, we presented the design, modeling, and experimental evaluation of a bio-inspired portable shoulder exoskeleton with cable-driven quasi-direct-drive (C-QDD) actuation that can compensate joint misalignment and mitigate interference between robot and human natural movements. Our biomimetic self-aligning mechanism design enabled effective shoulder assistance without joint misalignment by mimicking

the kinematics of human scapula movement during shoulder lifting. The variable lever arm mechanism reduced the bulkiness of the transmission structure moving with upper arm to mitigate physical interference between the robot and natural shoulder range of motion. Our simplified mechanism further exemplifies the “less-is-more” design philosophy that reduces interference with natural movement and preserves natural motion. The actuation paradigm of cable-driven quasi-direct drive (QDD) actuation enabled the creation of a fully portable, lightweight shoulder exoskeleton that can provide human-scale torque assistance. Benchtop test results show that our robot can provide assistive torque up to 13 Nm with a variable moment arm that increases linearly as the shoulder elevates. Human subject tests demonstrated that our robot 1) preserved most of the shoulder joint natural movement with less than 8% reduction in range of motion; 2) significantly reduced muscle activity, particularly in the anterior and medial deltoid muscles, which achieved the highest net muscle activation reduction during overhead assembly, lifting, and holding tasks compared to state-of-the-art results. 3) provided effective torque assistance in both shoulder flexion and abduction, enabling upper limb movement assistance for a wide range of activities of daily living. Importantly, our findings show that effective assistance can be achieved without design complexity. A simple gravity compensation controller, paired with our biomimetic robot design, delivered torque support up to 13 Nm while preserving natural shoulder kinematics. The human subject experiments demonstrated substantial reductions in muscular effort and minimal restriction in range of motion. Future work will involve long-term evaluations of the exoskeleton with diverse users in real-world scenarios, like manufacturing plants and retail stores, to assess its potential for reducing shoulder fatigue, mitigating musculoskeletal disorders, improving performance in workplace and daily use settings, and expanding employment and earnings for people with disabilities.

REFERENCES

- [1] M. Xiloyannis, R. Alicea, A.-M. Georgarakis, F. L. Haufe, P. Wolf, L. Masia, and R. Riener, “Soft robotic suits: State of the art, core technologies, and open challenges,” *IEEE Transactions on Robotics*, vol. 38, no. 3, pp. 1343–1362, 2021.
- [2] S. Crea, P. Beckerle, M. De Looze, K. De Pauw, L. Grazi, T. Kermavnar, J. Masood, L. W. O’Sullivan, I. Pacifico, C. Rodriguez-Guerrero et al., “Occupational exoskeletons: A roadmap toward large-scale adoption, methodology and challenges of bringing exoskeletons to workplaces,” *Wearable Technologies*, vol. 2, p. e11, 2021.
- [3] M. Ameri and T. Kurtzberg, “Neat gizmo! that looks scary: employer reactions to assistive technology,” *Journal of Occupational Rehabilitation*, vol. 34, no. 2, pp. 316–326, 2024.
- [4] D. Kruse, L. Schur, H.-A. Johnson-Marcus, L. Gilbert, A. Di Lallo, W. Gao, and H. Su, “Assistive technology’s potential to improve employment of people with disabilities,” *Journal of Occupational Rehabilitation*, pp. 1–17, 2024.
- [5] A. Gupta and M. K. O’Malley, “Robotic exoskeletons for upper extremity rehabilitation,” *Rehabilitation Robotics*, vol. 10, p. 5171, 2007.
- [6] N. Rehmat, J. Zuo, W. Meng, Q. Liu, S. Q. Xie, and H. Liang, “Upper limb rehabilitation using robotic exoskeleton systems: A systematic review,” *International Journal of Intelligent Robotics and Applications*, vol. 2, pp. 283–295, 2018.
- [7] Y. Zimmermann, M. Sommerhalder, P. Wolf, R. Riener, and M. Hutter, “Anyexo 2.0: A fully actuated upper-limb exoskeleton for manipulation and joint-oriented training in all stages of rehabilitation,” *IEEE Transactions on Robotics*, vol. 39, no. 3, pp. 2131–2150, 2023.
- [8] S. Han, H. Wang, and H. Yu, “Human–robot interaction evaluation-based gain control for upper limb rehabilitation robots driven by series elastic actuators,” *IEEE Transactions on Robotics*, 2023.
- [9] D. Zanotto, Y. Akiyama, P. Stegall, and S. K. Agrawal, “Knee joint misalignment in exoskeletons for the lower extremities: Effects on user’s gait,” *IEEE Transactions on Robotics*, vol. 31, no. 4, pp. 978–987, 2015.
- [10] L.-R. Chang, P. Anand, and M. Varacallo, “Anatomy, shoulder and upper limb, glenohumeral joint,” in *StatPearls [Internet]*. StatPearls Publishing, 2023.
- [11] M. A. Gull, S. Bai, and T. Bak, “A review on design of upper limb exoskeletons,” *Robotics*, vol. 9, no. 1, p. 16, 2020.
- [12] H. Veeger and F. Van Der Helm, “Shoulder function: the perfect compromise between mobility and stability,” *Journal of biomechanics*, vol. 40, no. 10, pp. 2119–2129, 2007.
- [13] D. Park, S. Toxiri, G. Chini, C. Di Natali, D. G. Caldwell, and J. Ortiz, “Shoulder-sidewinder (shoulder-side wearable industrial ergonomic robot): Design and evaluation of shoulder wearable robot with mechanisms to compensate for joint misalignment,” *IEEE Transactions on Robotics*, vol. 38, no. 3, pp. 1460–1471, 2021.
- [14] Y. M. Zhou, C. J. Hohimer, H. T. Young, C. M. McCann, D. Pont-Esteban, U. S. Civici, Y. Jin, P. Murphy, D. Wagner, T. Cole et al., “A portable inflatable soft wearable robot to assist the shoulder during industrial work,” *Science Robotics*, vol. 9, no. 91, p. eadi2377, 2024.
- [15] W. Qian, J. Liao, L. Lu, L. Ai, M. Li, X. Xiao, and Z. Guo, “Curer: A lightweight cable-driven compliant upper limb rehabilitation exoskeleton robot,” *IEEE/ASME Transactions on Mechatronics*, vol. 28, no. 3, pp. 1730–1741, 2022.
- [16] S. Ding, A. Narayan, F. A. Reyes, S. Han, and H. Yu, “Design and control of a novel active shoulder exoskeleton for overhead work assistance,” *IEEE/ASME Transactions on Mechatronics*, 2024.
- [17] A.-M. Georgarakis, M. Xiloyannis, P. Wolf, and R. Riener, “A textile exomuscle that assists the shoulder during functional movements for everyday life,” *Nature Machine Intelligence*, vol. 4, no. 6, pp. 574–582, 2022.
- [18] A. Ebrahimi, “Stuttgart exo-jacket: An exoskeleton for industrial upper body applications,” in *2017 10th International Conference on Human System Interactions (HSI)*. IEEE, 2017, pp. 258–263.
- [19] A. Otten, C. Voort, A. Stienen, R. Aarts, E. van Asseldonk, and H. van der Kooij, “Limpact: A hydraulically powered self-aligning upper limb exoskeleton,” *IEEE/ASME transactions on mechatronics*, vol. 20, no. 5, pp. 2285–2298, 2015.
- [20] S. Bai, S. Christensen, and M. R. U. Islam, “An upper-body exoskeleton with a novel shoulder mechanism for assistive applications,” in *2017 IEEE international conference on advanced intelligent mechatronics (AIM)*. IEEE, 2017, pp. 1041–1046.
- [21] G. Rinaldi, L. Tiseni, M. Xiloyannis, L. Masia, A. Frisoli, and D. Chiariadina, “Flexos: A portable, sea-based shoulder exoskeleton with hyper-redundant kinematics for weight lifting assistance,” in *2023 IEEE World Haptics Conference (WHC)*. IEEE, 2023, pp. 252–258.
- [22] L. Tiseni, M. Xiloyannis, D. Chiariadina, N. Lotti, M. Solazzi, H. Van der Kooij, A. Frisoli, and L. Masia, “On the edge between soft and rigid: an assistive shoulder exoskeleton with hyper-redundant kinematics,” in *2019 IEEE 16th International Conference on Rehabilitation Robotics (ICORR)*. IEEE, 2019, pp. 618–624.
- [23] B. Kim and A. D. Deshpande, “An upper-body rehabilitation exoskeleton harmony with an anatomical shoulder mechanism: Design, modeling, control, and performance evaluation,” *The International Journal of Robotics Research*, vol. 36, no. 4, pp. 414–435, 2017.
- [24] N. Li, T. Yang, P. Yu, J. Chang, L. Zhao, X. Zhao, I. H. Elhajj, N. Xi, and L. Liu, “Bio-inspired upper limb soft exoskeleton to reduce stroke-induced complications,” *Bioinspiration & biomimetics*, vol. 13, no. 6, p. 066001, 2018.
- [25] M. B. Yandell, D. M. Ziemnicki, K. A. McDonald, and K. E. Zelik, “Characterizing the comfort limits of forces applied to the shoulders, thigh and shank to inform exosuit design,” *PloS one*, vol. 15, no. 2, p. e0228536, 2020.
- [26] H. T. Peters, S. J. Page, and A. Persch, “Giving them a hand: wearing a myoelectric elbow-wrist-hand orthosis reduces upper extremity impairment in chronic stroke,” *Archives of physical medicine and rehabilitation*, vol. 98, no. 9, pp. 1821–1827, 2017.
- [27] C. Simpson, B. Huerta, S. Sketch, M. Lansberg, E. Hawkes, and A. Okamura, “Upper extremity exomuscle for shoulder abduction support,” *IEEE Transactions on Medical Robotics and Bionics*, vol. 2, no. 3, pp. 474–484, 2020.
- [28] T. Proietti, C. O’Neill, L. Gerez, T. Cole, S. Mendelowitz, K. Nuckols, C. Hohimer, D. Lin, S. Paganoni, and C. Walsh, “Restoring arm function with a soft robotic wearable for individuals with amyotrophic lateral

- sclerosis," *Science Translational Medicine*, vol. 15, no. 681, p. eadd1504, 2023.
- [29] E. Ricard, C. Hayot, I. Clerc-Urmès, L. Claudon, K. Desbrosses, and C. Pontonnier, "Evaluation of the static and dynamic assistive torque of a passive upper limb occupational exoskeleton," *Wearable Technologies*, vol. 6, p. e19, 2025.
- [30] S. Luo, M. Jiang, S. Zhang, J. Zhu, S. Yu, I. Dominguez Silva, T. Wang, E. Rouse, B. Zhou, H. Yuk, X. Zhou, and H. Su, "Experiment-free exoskeleton assistance via learning in simulation," *Nature*, vol. 630, no. 8016, pp. 353–359, 2024.
- [31] M. P. De Looze, T. Bosch, F. Krause, K. S. Stadler, and L. W. O'sullivan, "Exoskeletons for industrial application and their potential effects on physical work load," *Ergonomics*, vol. 59, no. 5, pp. 671–681, 2016.
- [32] J. Howard, V. Murashov, B. D. Lowe, and J. Lu. (2020) Industrial exoskeletons. Accessed: 2024-09-10. [Online]. Available: <https://blogs.cdc.gov/niosh-science-blog/2020/01/07/industrial-exoskeletons/>
- [33] B. D. Lowe, R. B. Dick, S. Hudock, and T. Bobick. (2022) Wearable exoskeletons to reduce physical load at work. Accessed: 2024-09-10. [Online]. Available: <https://blogs.cdc.gov/niosh-science-blog/2016/03/04/exoskeletons/>
- [34] S. De Bock, M. Rossini, D. Lefebvre, C. Rodriguez-Guerrero, J. Geeroms, R. Meeusen, and K. De Pauw, "An occupational shoulder exoskeleton reduces muscle activity and fatigue during overhead work," *IEEE Transactions on Biomedical Engineering*, vol. 69, no. 10, pp. 3008–3020, 2022.
- [35] Comau. (2024) Wearable robotics exoskeletons. Accessed: 2024-08-16. [Online]. Available: <https://www.comau.com/en/our-offer/products-and-solutions/wearable-robotics-exoskeletons/>
- [36] Crimson. (2025) Wearable robotics exoskeletons. Accessed: 2025-07-06. [Online]. Available: <https://www.c-dyn.com/en/h-col-134.html>
- [37] M. Xu, Z. Zhou, Z. Wang, L. Ruan, J. Mai, and Q. Wang, "Bio-inspired cable-driven actuation system for wearable robotic devices: Design, control and characterization," *IEEE Transactions on Robotics*, 2023.
- [38] C. O'Neill, T. Proietti, K. Nuckols, M. E. Clarke, C. J. Hohimer, A. Cloutier, D. J. Lin, and C. J. Walsh, "Inflatable soft wearable robot for reducing therapist fatigue during upper extremity rehabilitation in severe stroke," *IEEE Robotics and Automation Letters*, vol. 5, no. 3, pp. 3899–3906, 2020.
- [39] D. Park, C. Di Natali, D. G. Caldwell, and J. Ortiz, "Control strategy for shoulder-sidewinder with kinematics, load estimation, and friction compensation: Preliminary validation," *IEEE Robotics and Automation Letters*, vol. 7, no. 2, pp. 1278–1283, 2021.
- [40] S. Yu, T.-H. Huang, X. Yang, C. Jiao, J. Yang, Y. Chen, J. Yi, and H. Su, "Quasi-direct drive actuation for a lightweight hip exoskeleton with high backdrivability and high bandwidth," *IEEE/ASME Transactions on Mechatronics*, vol. 25, no. 4, pp. 1794–1802, 2020.
- [41] A. Engin and S.-M. Chen, "Statistical data base for the biomechanical properties of the human shoulder complex—ii: Passive resistive properties beyond the shoulder complex sinus," *Journal of Biomechanical Engineering*, 1986.
- [42] P. De Leva, "Adjustments to zatsiorsky-seluyanov's segment inertia parameters," *Journal of biomechanics*, vol. 29, no. 9, pp. 1223–1230, 1996.
- [43] S. Plagenhoef, F. G. Evans, and T. Abdelnour, "Anatomical data for analyzing human motion," *Research quarterly for exercise and sport*, vol. 54, no. 2, pp. 169–178, 1983.
- [44] J. C. Perry, J. Rosen, and S. Burns, "Upper-limb powered exoskeleton design," *IEEE/ASME transactions on mechatronics*, vol. 12, no. 4, pp. 408–417, 2007.
- [45] P. W. Franks, G. M. Bryan, R. M. Martin, R. Reyes, A. C. Lakmazaheri, and S. H. Collins, "Comparing optimized exoskeleton assistance of the hip, knee, and ankle in single and multi-joint configurations," *Wearable Technologies*, vol. 2, p. e16, 2021.
- [46] V. Nalam, X. Tu, M. Li, J. Si, and H. H. Huang, "Admittance control based human-in-the-loop optimization for hip exoskeleton reduces human exertion during walking," in *2022 International Conference on Robotics and Automation (ICRA)*. IEEE, 2022, pp. 6743–6749.
- [47] T. Proietti, E. Ambrosini, A. Pedrocchi, and S. Micera, "Wearable robotics for impaired upper-limb assistance and rehabilitation: State of the art and future perspectives," *Ieee Access*, vol. 10, pp. 106117–106134, 2022.
- [48] D. H. Gates, L. S. Walters, J. Cowley, J. M. Wilken, and L. Resnik, "Range of motion requirements for upper-limb activities of daily living," *The American journal of occupational therapy*, vol. 70, no. 1, pp. 7001350010p1–7001350010p10, 2016.
- [49] I. Pacifico, A. Scano, E. Guanziroli, M. Moise, L. Morelli, A. Chiavenna, D. Romo, S. Spada, G. Colombina, F. Molteni et al., "An experimental evaluation of the proto-mate: a novel ergonomic upper-limb exoskeleton to reduce workers' physical strain," *IEEE robotics & automation magazine*, vol. 27, no. 1, pp. 54–65, 2020.
- [50] D. Magermans, E. Chadwick, H. Veeger, and F. Van Der Helm, "Requirements for upper extremity motions during activities of daily living," *Clinical biomechanics*, vol. 20, no. 6, pp. 591–599, 2005.
- [51] J. Aizawa, T. Masuda, T. Koyama, K. Nakamaru, K. Isozaki, A. Okawa, and S. Morita, "Three-dimensional motion of the upper extremity joints during various activities of daily living," *Journal of biomechanics*, vol. 43, no. 15, pp. 2915–2922, 2010.
- [52] S. Namdari, G. Yagnik, D. D. Ebaugh, S. Nagda, M. L. Ramsey, G. R. Williams Jr, and S. Mehta, "Defining functional shoulder range of motion for activities of daily living," *Journal of shoulder and elbow surgery*, vol. 21, no. 9, pp. 1177–1183, 2012.
- [53] H. J. Hermens, B. Freriks, C. Disselhorst-Klug, and G. Rau, "Development of recommendations for semg sensors and sensor placement procedures," *Journal of electromyography and Kinesiology*, vol. 10, no. 5, pp. 361–374, 2000.
- [54] J. Brooke et al., "Sus-a quick and dirty usability scale," *Usability evaluation in industry*, vol. 189, no. 194, pp. 4–7, 1996.
- [55] G. A. Borg, "Psychophysical bases of perceived exertion," *Medicine and science in sports and exercise*, vol. 14, no. 5, pp. 377–381, 1982.
- [56] G. Borg, "Perceived exertion as an indicator of somatic stress," *Scandinavian journal of rehabilitation medicine*, 1970.
- [57] M. Rossini, S. De Bock, A. van der Have, L. Flynn, D. Rodriguez-Cianca, K. De Pauw, D. Lefebvre, J. Geeroms, and C. Rodriguez-Guerrero, "Design and evaluation of a passive cable-driven occupational shoulder exoskeleton," *IEEE Transactions on Medical Robotics and Bionics*, vol. 3, no. 4, pp. 1020–1031, 2021.
- [58] Y. Ding, M. Kim, S. Kuindersma, and C. J. Walsh, "Human-in-the-loop optimization of hip assistance with a soft exosuit during walking," *Science robotics*, vol. 3, no. 15, p. eaar5438, 2018.